

Cite this: *Phys. Chem. Chem. Phys.*,  
2014, 16, 3399

# Infrared and reflectron time-of-flight mass spectroscopic analysis of methane (CH<sub>4</sub>)–carbon monoxide (CO) ices exposed to ionization radiation – toward the formation of carbonyl-bearing molecules in extraterrestrial ices†

Ralf I. Kaiser,<sup>\*ab</sup> Surajit Maity<sup>ab</sup> and Brant M. Jones<sup>\*ab</sup>

Ice mixtures of methane and carbon monoxide were exposed to ionizing radiation in the form of energetic electrons at 5.5 K to investigate the formation of carbonyl bearing molecules in extraterrestrial ices. The radiation induced chemical processing of the mixed ices along with their isotopically labeled counterparts was probed online and *in situ* via infrared spectroscopy (solid state) aided with reflectron time-of-flight mass spectrometry (ReTOFMS) coupled to single photon photoionization (PI) at 10.49 eV (gas phase). Deconvolution of the carbonyl absorption feature centered at 1727 cm<sup>-1</sup> in the processed ices and subsequent kinetic fitting to the temporal growth of the newly formed species suggests the formation of acetaldehyde (CH<sub>3</sub>CHO) together with four key classes of carbonyl-bearing molecules: (i) alkyl aldehydes, (ii) alkyl ketones, (iii)  $\alpha,\beta$ -unsaturated ketones/aldehydes and (iv)  $\alpha,\beta,\gamma,\delta$ -unsaturated ketones/ $\alpha,\beta$ -dicarbonyl compounds in keto-enol form. The mechanistical studies indicate that acetaldehyde acts as the key building block of higher aldehydes (i) and ketones (ii) with unsaturated ketones/aldehydes (iii) and/or  $\alpha,\beta$ -dicarbonyl compounds (iv) formed from the latter. Upon sublimation of the newly synthesized molecules, ReTOFMS together with isotopic shifts of the mass-to-charge ratios was exploited to identify eleven product classes containing molecules with up to six carbon atoms, which can be formally derived from C1–C5 hydrocarbons incorporating up to three carbon monoxide building blocks. The classes are (i) saturated aldehydes/ketones, (ii) unsaturated aldehydes/ketones, (iii) doubly unsaturated aldehydes/ketones, (iv) saturated dicarbonyls (aldehydes/ketones), (v) unsaturated dicarbonyls (aldehydes/ketones), (vi) saturated tricarbonyls (aldehydes/ketones), molecules containing (vii) one carbonyl – one alcohol (viii), two carbonyls – one alcohol, (ix) one carbonyl – two alcohol groups along with (x) alcohols and (xi) diols. Reaction pathways to synthesize these classes were derived as well. The present experiments provide clear evidence for the formation of key organic molecules – acetaldehyde, acetone, and potentially vinylalcohol – which are among the 15 carbonyl containing organic molecules detected in the interstellar medium. Despite numerous previous experimental investigations probing the effect of ionizing radiation on simple astrophysical ice representatives, our results suggest that more complex organic molecules can be formed in extraterrestrial ices than previously suggested. An outlook on further identification of individual isomers is also presented.

Received 9th October 2013,  
Accepted 6th November 2013

DOI: 10.1039/c3cp54255f

www.rsc.org/pccp

## 1. Introduction

During the last decade, astronomical observations of simple carbonyl-bearing molecules in the interstellar medium (ISM)

such as acetaldehyde (CH<sub>3</sub>CHO), glycolaldehyde (HCOCH<sub>2</sub>OH), methyl formate (HCOOCH<sub>3</sub>), and acetic acid (CH<sub>3</sub>COOH) have received considerable interest from the astrochemistry and astrobiology communities<sup>1–6</sup> because these molecules are considered as key precursors of biologically important molecules such as carbohydrates,<sup>7</sup> amino acids, and polypeptides.<sup>3,8</sup> As the simplest representative of a closed-shell aldehyde, acetaldehyde has emerged as a benchmark molecule since its detection in Sagittarius B2 to understand the astrochemical evolution of cold molecular clouds and of star forming regions.<sup>9</sup> It became quite clear that acetaldehyde is ubiquitous

<sup>a</sup> W. M. Keck Research Laboratory in Astrochemistry,  
University of Hawaii at Manoa, Honolulu, Hawaii, HI 96822, USA  
<sup>b</sup> Department of Chemistry, University of Hawaii at Manoa, Honolulu, Hawaii,  
HI 96822, USA

† This Article is Published in Celebration of the 50th Anniversary of the Opening of the Chemistry Department at the University of York.

in the interstellar medium as it was observed in cold molecular clouds (TMC-1,<sup>10,11</sup> L134N<sup>12</sup>), hot cores and star forming regions (Sgr B2,<sup>13</sup> NGC 6334F, Orion Compact Ridge<sup>14–18</sup>), and translucent clouds (CB 17, CB 24, CB 228).<sup>19,20</sup> In addition, glycolaldehyde (HCOCH<sub>2</sub>OH) – the simplest carbohydrate – was identified in Sgr B2(N)-LMH<sup>21,22</sup> and in the hot molecular core G31.41 + 0.31.<sup>23</sup> Further, acetone (CH<sub>3</sub>COCH<sub>3</sub>) was found in star-forming regions Sgr B2<sup>24</sup> and Orion-KL;<sup>25</sup> the existence of higher aldehydes such as propenal (CH<sub>2</sub>CHCHO) and propanal (CH<sub>3</sub>CH<sub>2</sub>CHO) was confirmed *via* their detection in Sgr B2(N).<sup>26</sup>

Despite the importance of acetaldehyde (CH<sub>3</sub>CHO) as an evolutionary tracer in astrochemistry and astrobiology,<sup>2,15,27,28,29</sup> the underlying formation routes remain mainly inconclusive and cannot be explained by networks of gas phase ion-molecule reactions.<sup>20,30</sup> Here, the modeled abundances in star forming regions such as Sgr B2 were three orders of magnitude less than those derived from the actual observations depicting fractional abundances of about 10<sup>−9</sup> obtained from the Nobeyama Radio Observatory (NRO) and Swedish-ESO Submillimetre Telescope (SEST).<sup>31</sup> Therefore, a source providing acetaldehyde is missing. Subsequent models attempted to boost the production rates of acetaldehyde by incorporating grain-surface chemistry involving radical-radical reactions on interstellar grains.<sup>32</sup> These models also failed to explain the observed abundance of acetaldehyde.<sup>33</sup> The inadequate agreement between modeled and observed abundances is based on the fact that current astrochemical models disregard the chemical processing of the ‘bulk’ ice mantle of interstellar grains by ionizing radiation and only consider the grain surface. Here, interstellar grains have been found to be coated with an icy ‘mantle’ consisting mainly of water (H<sub>2</sub>O) followed by methanol (CH<sub>3</sub>OH), carbon monoxide (CO), carbon dioxide (CO<sub>2</sub>), methane (CH<sub>4</sub>), ammonia (NH<sub>3</sub>), and formaldehyde (H<sub>2</sub>CO) having thicknesses of up to a few hundred nanometers.<sup>34–36</sup> The interaction of these ices with galactic cosmic rays (GCRs) and with the internal ultraviolet field inside cold molecular clouds has repeatedly been demonstrated to chemically modify the pristine ices *via* non-thermal, non-equilibrium chemistry involving supra-thermal reactants such as hydrogen, oxygen, nitrogen, and carbon atoms, which are not in thermal equilibrium with the 10 K ices.<sup>20,37–42</sup> Therefore, in cold molecular clouds, an interaction of ionizing radiation with ice coated nanoparticles is expected to lead to the synthesis of complex organic molecules, which cannot be explained by classical thermal reactions; once the molecular cloud collapses and transforms into star-forming regions, the elevated temperatures of up to about 250 K result in sublimation of these newly formed organic molecules, which are then monitored by radio astronomy. Note that both methane (CH<sub>4</sub>) and carbon monoxide (CO) have been observed in 18 out of 23 young stellar objects (YSO) exploiting the Infrared Space Observatory. The simultaneous detection of acetaldehyde (CH<sub>3</sub>CHO) in 12 of these 18 objects<sup>36</sup> strongly suggests that acetaldehyde can be synthesized on icy grains containing methane and carbon monoxide subjected to ionizing radiation followed by sublimation into the gas phase.

Preliminary laboratory experiments propose that acetaldehyde can be formed in binary ice mixtures of methane-carbon

monoxide (CH<sub>4</sub>-CO),<sup>43</sup> carbon dioxide-ethylene (CO<sub>2</sub>-C<sub>2</sub>H<sub>4</sub>),<sup>44</sup> methanol-carbon monoxide (CH<sub>3</sub>OH-CO),<sup>6</sup> and methane-carbon dioxide (CH<sub>4</sub>-CO<sub>2</sub>) involving suprathreshold (non-equilibrium) chemistry.<sup>5</sup> Here, reactions of suprathreshold hydrogen atoms, for instance, can be multiple orders of magnitude faster than those of their thermal counterparts and can even overcome entrance barriers to addition of double and triple bonds.<sup>45</sup> A recent study by Ward *et al.* revealed that acetaldehyde might also be synthesized from reactions of ethylene (C<sub>2</sub>H<sub>4</sub>) with thermal oxygen atoms at 12–90 K.<sup>46</sup> Currently, the only mechanistical study focused on the effects of ionizing radiation in terms of energetic electrons as formed in the track of galactic cosmic ray particles in methane-carbon monoxide ices at 10 K. At an average dose of 1.1 ± 0.2 eV per molecule, three key species were identified: the methyl radical (CH<sub>3</sub>), the formyl radical (HCO), and acetaldehyde (CH<sub>3</sub>CHO). Based on the temporal evolution of the column densities of these species during the irradiation, acetaldehyde was suggested to be formed *via* the radical-radical reaction of methyl (CH<sub>3</sub>) and formyl (HCO) at 10 K within the matrix cage.<sup>43</sup> Upon warming up of the irradiated samples, methyl and formyl radicals can also diffuse and recombine forming further acetaldehyde molecules. Therefore, both the astronomical observations and laboratory studies demonstrated that radiation exposure of ‘bulk’ ices containing methane and carbon monoxide, but not grain-surface reactions, leads to the synthesis of acetaldehyde in the interstellar medium. However, with the exception of formaldehyde, acetaldehyde was the only aldehyde identified in previous irradiation experiments; the asymmetric shape of the infrared absorption in the region of 1727 cm<sup>−1</sup> hints at the formation of more complex carbonyl-bearing molecules. Likewise, mass spectroscopic data indicate that more complex organic molecules carrying the carbonyl functional group are synthesized. Here, acetaldehyde could not be monitored *via* its *m/z* = 44 parent peak due to interference from carbon dioxide (CO<sub>2</sub>) and propane (C<sub>3</sub>H<sub>8</sub>), which were also produced in the irradiation of methane-carbon monoxide ices. Therefore, acetaldehyde was observed *via* its *m/z* = 43 fragment ion (CH<sub>3</sub>CO<sup>+</sup>). However, this fragment, which is formed *via* α-cleavage of the parent ion, is also characteristic of methyl ketones. The temperature dependent ion current of *m/z* = 43 depicted multiple peaks suggesting the synthesis of more complex carbonyl-bearing molecules, possibly methylketones. However, the nature of these species has remained elusive so far.

A recent experiment on the irradiation products of pure methane ices exploited a novel technique in space simulation experiments. Jones *et al.* demonstrated that the formation of complex hydrocarbons as large as C<sub>22</sub>H<sub>2n+2</sub> can be elucidated utilizing reflectron time-of-flight mass spectrometry (ReTOFMS) coupled with single photon photoionization (ReTOFMS-PI).<sup>47</sup> Whereas these high-mass hydrocarbons were masked within the infrared spectra due to similar vibrational group frequencies and exceedingly low column densities, ReTOFMS coupled with single photon vacuum ultraviolet photoionization (ReTOFMS-PI; *E<sub>hν</sub>* = 10.49 eV) was exploited to discriminate between alkanes, alkenes, and even dienes/alkynes; note that this identification could not have been achieved *via* conventional mass spectrometers utilizing electron impact ionization since alkanes such

as pentane (C<sub>5</sub>H<sub>12</sub>) depict fragment ions of identical mass-to-charge ratios as parent ions of unsaturated hydrocarbons such as alkenes like pentene (C<sub>5</sub>H<sub>10</sub>). Due to the success of the ReTOFMS-PI approach in identifying hitherto unobserved, astrochemically relevant molecules in irradiated methane samples, we are presenting here a detailed study on the interaction of energetic electrons with interstellar analog ices of methane–carbon monoxide (CH<sub>4</sub>–CO) in an attempt to elucidate the formation of carbonyl-bearing organic molecules in cold molecular clouds on icy grains, thus providing us for the very first time the nature of complex, novel reaction products of processed methane–carbon monoxide ices.

## 2. Experimental section

The experiments were carried out in a contamination-free ultrahigh vacuum (UHV) chamber evacuated to a base pressure of typically  $2 \times 10^{-11}$  Torr by three magnetically suspended turbo molecular pumps backed by an oil free scroll pump.<sup>47,48</sup> Briefly, a silver mirror, interfaced with a closed-cycle helium refrigerator and a programmable temperature controller, is positioned inside the UHV chamber and is freely rotatable within the horizontal center plane of the chamber. The silver mirror acts as a substrate and is cooled down to  $5.5 \pm 0.1$  K. Premixed gases of methane (CH<sub>4</sub>, Specialty Gases of America, 99.999%) and carbon monoxide (CO, Aldrich, 99.99%) with partial pressures of 100 Torr and 130 Torr, respectively, were then introduced into the main chamber through a glass capillary array held 30 mm in front of the silver mirror at a pressure of  $5 \times 10^{-8}$  Torr for approximately 3 min. The ice thickness was determined online and *in situ via* laser interferometry to be  $520 \pm 20$  nm utilizing an index of refraction of the mixed ice of  $1.31 \pm 0.02$  at a helium–neon (HeNe) laser wavelength of 632.8 nm derived from numerical fitting of the observed intensity ratios.<sup>49</sup> Laser interferometry can only determine the total thickness of the ices, but not the ratio of the methane to carbon monoxide deposited. Here, the ratio of the ice composition of methane to carbon monoxide of  $3.5 \pm 0.5 : 2.5 \pm 0.5$  was derived by calculating the column densities of the methane and carbon monoxide utilizing modified Lambert–Beer relationship<sup>50–52</sup> with the absorption coefficients of  $3.5 \times 10^{-19}$  cm molecule<sup>-1</sup> and  $1.1 \times 10^{-17}$  cm molecule<sup>-1</sup> for the  $4204 \text{ cm}^{-1}$  ( $\nu_1 + \nu_4$ ; CH<sub>4</sub>) and the  $2090 \text{ cm}^{-1}$  ( $\nu_1$ ; <sup>13</sup>CO) bands, respectively.<sup>39,53</sup> Isotopically mixed ices of CD<sub>4</sub>–CO, CD<sub>4</sub>–<sup>13</sup>CO, and CH<sub>4</sub>–C<sup>18</sup>O (CD<sub>4</sub>, CDN Isotopes, 99.9% D; <sup>13</sup>CO, Aldrich, 99% <sup>13</sup>C; C<sup>18</sup>O, Aldrich, 99% <sup>18</sup>O) were also produced to confirm infrared assignments *via* isotope shifts and ReTOFMS-PI data *via* their shifts in mass-to-charge ratios. The ices were then irradiated with 5 keV electrons isothermally at  $5.5 \pm 0.1$  K for one hour at 30 nA over an area of  $1.0 \pm 0.1$  cm<sup>2</sup> and an angle of incidence of 70° relative to the surface normal of the ice. The average dose [ $1.4 \pm 0.3$  eV per 16 amu;  $5.1 \pm 1.3$  eV per CO molecule;  $4.7 \text{ eV} \pm 1.4$  per CH<sub>4</sub> molecule] deposited into the samples was determined *via* Monte Carlo (CASINO) simulations.<sup>54</sup> The applied dose corresponds to approximately 10<sup>5</sup> years in cold molecular clouds.<sup>55</sup> Note that the calculated penetration depth of the energetic electrons of

380 nm is less than the thickness of the sample of  $520 \pm 20$  nm. Therefore, the electrons only interact with the ice and not with the silver substrate.

The irradiation-induced chemical processing of the ices was monitored online and *in situ via* a Fourier Transform Infrared Spectrometer (Nicolet 6700) over a range of 6000 to 400 cm<sup>-1</sup> at a resolution of 4 cm<sup>-1</sup>. Each FTIR spectrum was recorded in absorption–reflection–absorption mode (reflection angle = 45°) for two minutes resulting in a set of 30 infrared spectra during the radiation exposure for each system. After the irradiation, the sample was kept at 5.5 K for one hour; then, temperature programmed desorption (TPD) studies were conducted by heating the irradiated ices at a rate of 0.5 K min<sup>-1</sup> to 300 K. The samples were also monitored *via* infrared spectroscopy. Further, the molecules subliming into the gas phase were probed *via* a quadrupole mass spectrometer (Extrel, Model 5221) operating in a residual-gas analyzer mode in the mass range of 1–500 amu with electron impact ionization at 100 eV and an emission current of 1 mA. In addition, the molecules were also monitored using a reflectron time-of-flight mass spectrometer (ReTOF) coupled with soft photoionization of the neutral molecules.<sup>47</sup> Here, the products were ionized upon sublimation *via single photon ionization* exploiting pulsed (30 Hz) coherent vacuum ultraviolet (VUV) light at 118.2 nm (10.49 eV). The third harmonic (354.6 nm) of a high-power pulsed Nd:YAG laser (Spectra Physics, PRO – 250; 30 mJ per pulse) was frequency tripled to produce the VUV photon utilizing xenon (Xe) gas as the nonlinear medium producing about 10<sup>13</sup> photons cm<sup>-2</sup> s<sup>-1</sup> depicting a conversion efficiency of about 10<sup>-4</sup>. A pulsed valve was housed in a doubly differentially pumped chamber held at typically  $2 \times 10^{-4}$  Torr when operated at 30 Hz, –400 V, and 80 μs opening time; the pulsed valve fired 200 μs prior to the Q-switch of the Nd:YAG laser to release the xenon gas at a backing pressure of 1266 Torr (99.999%; Specialty Gases of America) in a T-shaped stainless steel adapter with 1 mm diameter at 25 mm in length in line with the propagating laser beam (354.6 nm). The VUV light was then separated and directed to 1 mm above the ice surface utilizing an off-axis, differentially pumped lithium fluoride (LiF) lens,<sup>56</sup> where the sublimating molecules are then photoionized. The molecular ions were detected utilizing a multichannel plate with a dual chevron configuration and the signal amplified using a fast preamplifier (Ortec 9305) and shaped with a 100 MHz discriminator. The ions were mass resolved according to their arrival times. The ReTOF spectra were recorded with a personal-computer-based multichannel scaler (FAST ComTec, P7888-1 E) using a bin width of 4 ns, triggered at 30 Hz (Quantum Composers, 9518) with 3600 sweeps per mass spectrum correlated with a 1 K change in temperature.

## 3. Results and discussion

### 3.1. Infrared spectroscopy

**3.1.1. Qualitative analysis.** During the irradiation, multiple new absorption features emerged (Table 1 and Fig. 1). Most importantly, the formation of acetaldehyde (CH<sub>3</sub>CHO) was confirmed *via* the

detection of four absorptions at 1727 cm<sup>-1</sup> ( $\nu_4$ ), 1350 cm<sup>-1</sup> ( $\nu_7$ ), 1120 cm<sup>-1</sup> ( $\nu_8$ ), and 1427 cm<sup>-1</sup> ( $\nu_{12}$ ); these positions agree nicely with the data reported previously.<sup>43</sup> We also recorded a reference spectrum of 0.5% acetaldehyde in carbon monoxide–methane ices at 5.5 K and found that the acetaldehyde absorption in this mixture agrees nicely with that found in the irradiated sample (Table 1). Further, the methyl (CH<sub>3</sub>) radical was detected at 3151 cm<sup>-1</sup> ( $\nu_3$ ) and 613 cm<sup>-1</sup> ( $\nu_2$ )<sup>37,43</sup> along with the formyl radical (HCO) *via* its absorptions at 1853 cm<sup>-1</sup> ( $\nu_3$ ) and 1091 cm<sup>-1</sup> ( $\nu_2$ ).<sup>43</sup> Acetylene (C<sub>2</sub>H<sub>2</sub>) formation could be attributed *via* the 3253 cm<sup>-1</sup> band.<sup>57</sup> Ethylene (C<sub>2</sub>H<sub>4</sub>) was monitored *via* the position of the  $\nu_9$  fundamental at 3093 cm<sup>-1</sup>,<sup>57</sup> whereas ethane (C<sub>2</sub>H<sub>6</sub>) was assigned based on the bands at 2978 cm<sup>-1</sup> ( $\nu_{10}$ ), 2962 cm<sup>-1</sup> ( $\nu_1$ ), 2943 cm<sup>-1</sup>, 2920 cm<sup>-1</sup> ( $\nu_8 + \nu_{11}$ ), 2885 cm<sup>-1</sup> ( $\nu_5$ ), 1466 cm<sup>-1</sup> ( $\nu_{11}$ ) and 1373 cm<sup>-1</sup> ( $\nu_6$ ); these absorptions agree nicely with previous studies.<sup>37,57,58</sup> Formation of carbon dioxide can be traced *via* the 2341 cm<sup>-1</sup> band.<sup>50,59</sup> The assignments of the absorptions were confirmed *via* their isotopic shifts in CD<sub>4</sub>–CO, CD<sub>4</sub>-<sup>13</sup>CO, and CH<sub>4</sub>-C<sup>18</sup>O ices as compiled in Table 1.

It should be noted that the band at 1727 cm<sup>-1</sup> is broadened toward the low and high frequency sides. This finding suggests

the presence of multiple underlying carriers. Therefore, the ‘1727 cm<sup>-1</sup>’ feature was deconvoluted (Fig. 2 and Table 2). In the case of the methane–carbon monoxide ice, this procedure identified five bands at 1746 cm<sup>-1</sup>, 1727 cm<sup>-1</sup>, 1717 cm<sup>-1</sup>, 1701 cm<sup>-1</sup>, and 1660 cm<sup>-1</sup>. To correlate the band positions with possible carriers, deconvolution of the carbonyl features at 1700 cm<sup>-1</sup>, 1660 cm<sup>-1</sup>, and 1690 cm<sup>-1</sup> was also performed for the isotopically labeled ices CD<sub>4</sub>–CO, CD<sub>4</sub>-<sup>13</sup>CO, and CH<sub>4</sub>-C<sup>18</sup>O, respectively. A comparison of the extracted band positions with literature data proposes that the band at 1727 cm<sup>-1</sup> can be assigned to the  $\nu_4$  fundamental of acetaldehyde; this result is close to the literature values at 1728 cm<sup>-1</sup>.<sup>43,60,61</sup> The infrared absorption band at the high frequency side at 1746 cm<sup>-1</sup> can be assigned to saturated aldehydes with alkyl functional groups such as propanal (C<sub>2</sub>H<sub>5</sub>CHO) and butanal (n-C<sub>3</sub>H<sub>7</sub>CHO).<sup>62,63</sup> Here, absorptions of the carbonyl functional group were reported within 1740–1750 cm<sup>-1</sup> for a series of aldehydes with alkyl groups (C<sub>2</sub>H<sub>2n+1</sub>, n > 1) using matrix isolated FTIR spectroscopy. Further, the absorption feature at 1717 cm<sup>-1</sup> can be assigned to ketones with alkyl groups such as acetone (CH<sub>3</sub>COCH<sub>3</sub>). This assignment is based on previous

**Table 1** Infrared absorption features recorded before and after the irradiation of methane–carbon monoxide ices (CH<sub>4</sub>–CO, CD<sub>4</sub>–CO, CH<sub>4</sub>-C<sup>18</sup>O, CD<sub>4</sub>-<sup>13</sup>CO) at 5.5 K. Also compiled are infrared absorption features recorded in 0.5% acetaldehyde (CH<sub>3</sub>CHO) in CH<sub>4</sub>–CO ices (Fig. 1E)

CH <sub>4</sub> :CO		CD <sub>4</sub> :CO		CH <sub>4</sub> :C <sup>18</sup> O		CD <sub>4</sub> : <sup>13</sup> CO		0.5% CH <sub>3</sub> CHO in CH <sub>4</sub> :CO	Assignment	Carrier	Ref.
Before (cm <sup>-1</sup> )	After (cm <sup>-1</sup> )	Before (cm <sup>-1</sup> )	After (cm <sup>-1</sup> )	Before (cm <sup>-1</sup> )	After (cm <sup>-1</sup> )	Before (cm <sup>-1</sup> )	After (cm <sup>-1</sup> )				
—	—	4479	—	—	—	4479	—	—	2 $\nu_3$ (CD <sub>4</sub> )	Overtone	38
4534	—	—	—	4533	—	—	—	4532	$\nu_2 + \nu_3$ (CH <sub>4</sub> )	Combination	57
4302	—	3240	—	4303	—	3240	—	4302	$\nu_3 + \nu_4$ (CH <sub>4</sub> )	Combination	57
4248	—	4249	—	4148	—	4156	—	4248	2 $\nu_1$ (CO)	Overtone	68
4204	—	3090	—	4205	—	3090	—	4204	$\nu_1 + \nu_4$ (CH <sub>4</sub> )	Combination	57
—	3253	—	2445	—	3256	—	2445	—	$\nu_3$ (C <sub>2</sub> H <sub>2</sub> )	CH str.	38, 57
—	3151	—	2372	—	3151	—	—	—	$\nu_3$ (CH <sub>3</sub> )	CH str.	38, 43
—	3093	—	—	—	3095	—	—	—	$\nu_9$ (C <sub>2</sub> H <sub>4</sub> )	CH <sub>2</sub> asym. str.	57
3011	—	2252	—	3011	—	2252	—	3010	$\nu_3$ (CH <sub>4</sub> )	Deg. str.	38, 57
—	2978	—	2231	—	2978	—	2231	—	$\nu_{10}$ (C <sub>2</sub> H <sub>6</sub> )	CH <sub>3</sub> deg. str.	38, 57
—	—	—	—	—	—	—	—	2962	$\nu_{11}$ (CH <sub>3</sub> CHO)	CH <sub>3</sub> deg. str.	80
—	2962	—	2216	—	2961	—	2216	—	$\nu_1$ (C <sub>2</sub> H <sub>6</sub> )	CH <sub>3</sub> sym. str.	38, 57
—	2943	—	—	—	2942	—	—	—	$\nu_8 + \nu_{11}$ (C <sub>2</sub> H <sub>6</sub> )	Combination	38, 57
—	2920	—	2096	—	2918	—	—	—	$\nu_8 + \nu_{11}$ (C <sub>2</sub> H <sub>6</sub> )	Combination	38, 57
2905	—	2098	—	2905	—	—	—	2904	$\nu_1$ (CH <sub>4</sub> )	Sym. str.	38, 57
—	2885	—	2080	—	2885	—	—	—	$\nu_5$ (C <sub>2</sub> H <sub>6</sub> )	CH <sub>3</sub> sym. str.	38, 57
2818	—	—	—	2818	—	2063	—	2846, 2833, 2118	$\nu_2 + \nu_4$ (CH <sub>4</sub> )	Combination	38, 57
—	2748	—	1947	—	2742	—	1918	—	$\nu_2 + \nu_6$ (C <sub>2</sub> H <sub>6</sub> )	Combination	38, 57
2595	—	1978	—	2595	—	1979	—	2596	2 $\nu_4$ (CH <sub>4</sub> )	Overtone	38, 57
—	2341	—	2342	—	2339	—	2342	—	$\nu_6$ (CO <sub>2</sub> )	CO asym. str.	50
—	2276	—	2277	—	—	—	2276	—	$\nu_6$ ( <sup>13</sup> CO <sub>2</sub> )	CO asym. str.	50
—	—	—	—	—	2306	—	—	—	$\nu_6$ (C <sup>18</sup> O <sub>2</sub> )	CO asym. str.	—
—	—	—	—	—	2324	—	—	—	$\nu_6$ ( <sup>18</sup> OC <sup>16</sup> O)	CO asym. str.	—
—	—	2113	—	—	2108	—	2056	—	$\nu_2$ (CH <sub>3</sub> CO)	CO str.	79
2137	—	2137	—	2137	—	2137	—	2137	$\nu_1$ (CO)	CO str.	50, 68
2090	—	2091	—	2087	—	2089	—	2090	$\nu_1$ ( <sup>13</sup> CO)	CO str.	68
—	1853	—	1796	—	1810	—	1774	—	$\nu_2$ (HCO)	CO str.	43
—	1727	—	1717	—	1694	—	1669	1728	$\nu_4$ (CH <sub>3</sub> CHO)	CO str.	43
—	1466	—	—	—	1465	—	—	—	$\nu_{11}$ (C <sub>2</sub> H <sub>6</sub> )	CH <sub>3</sub> deform.	38, 57
—	1427	—	1024	—	1424	—	1022	1427	$\nu_{12}$ (CH <sub>3</sub> CHO)	CH <sub>3</sub> deform.	43
—	—	—	—	—	—	—	—	1402	$\nu_6$ (CH <sub>3</sub> CHO)	CH bend	80
—	1373	—	1052	—	—	—	1056	—	$\nu_6$ (C <sub>2</sub> H <sub>6</sub> )	CH <sub>3</sub> sym. deform.	38, 57
—	1350	—	1158	—	1349	—	1158	1348	$\nu_7$ (CH <sub>3</sub> CHO)	CH <sub>3</sub> deform.	43
1302	—	993	—	1302	—	992	—	1302	$\nu_4$ (CH <sub>4</sub> )	Deg. str.	38, 57
—	1120	—	1069	—	1120	—	1070	1117	$\nu_8$ (CH <sub>3</sub> CHO)	CH <sub>3</sub> deform.	43
—	1091	—	—	—	1089	—	—	—	$\nu_2$ (HCO)	Bending	43
—	613	—	—	—	—	—	—	—	$\nu_2$ (CH <sub>3</sub> )	Out of plane	38, 57



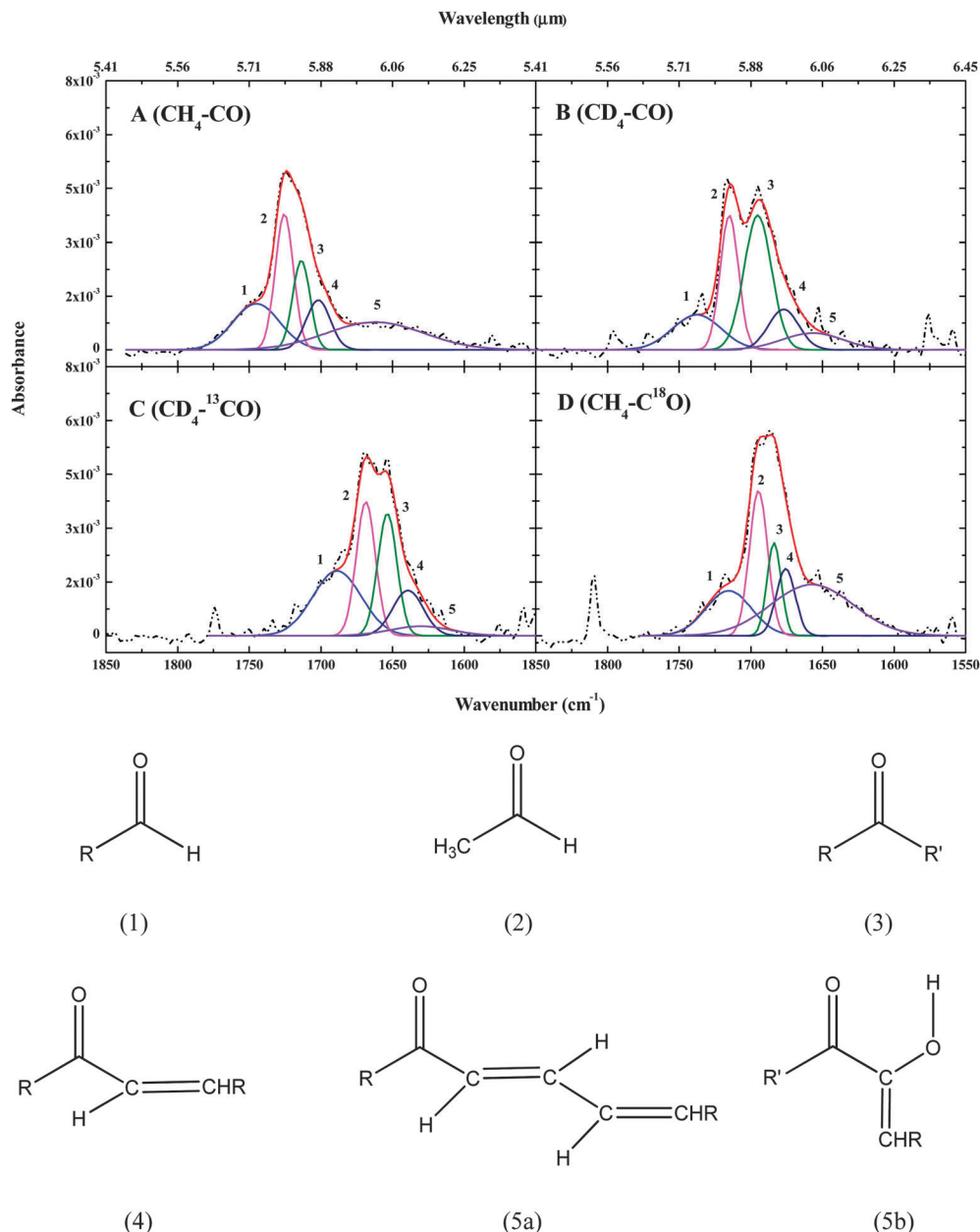


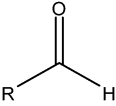
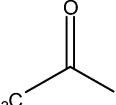
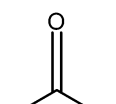
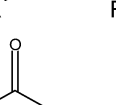
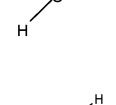
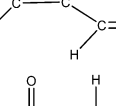
Fig. 2 Deconvoluted infrared absorption features in the region of the carbonyl functional group: (A)  $\text{CH}_4\text{-CO}$ , (B)  $\text{CD}_4\text{-CO}$ , (C)  $\text{CD}_4\text{-}^{13}\text{CO}$ , (D)  $\text{CH}_4\text{-C}^{18}\text{O}$  mixtures. The deconvolution results in five classes of molecules: (1) saturated aldehydes ( $\text{RCHO}$ ), (2) acetaldehyde ( $\text{CH}_3\text{CHO}$ ), (3) saturated ketones ( $\text{RCOR}'$ ), (4)  $\alpha,\beta$ -unsaturated aldehydes/ketones, and (5)  $\alpha,\beta,\gamma,\delta$ -unsaturated aldehydes/ketones (5a) and/or  $\alpha,\beta$ -dicarbonyl compounds in keto-enol form (5b). The generic molecular structures of these classes are also shown.

observations of matrix isolated acetone and  $\text{D}_6$ -acetone absorbing at  $1721\text{ cm}^{-1}$  and  $1708\text{ cm}^{-1}$  (ref. 64) in agreement with the observed values. However, ketones with higher alkyl groups such as ethyl and propyl can also contribute to this band.<sup>65</sup> The feature at  $1701\text{ cm}^{-1}$  can be assigned to  $\alpha,\beta$ -unsaturated aldehydes/ketones as a  $20\text{--}30\text{ cm}^{-1}$  redshift can be attributed to the  $\alpha,\beta$  unsaturation and hence lowering of the frequency due to resonance.<sup>66</sup> Finally, the broad infrared absorption band at  $1660\text{ cm}^{-1}$  can be linked to  $\alpha,\beta$ -dicarbonyl compounds in keto-enol form,  $\alpha,\beta,\gamma,\delta$ -unsaturated aldehydes/ketones, and a combination of both, *i.e.* unsaturated dicarbonyls; note that

higher carbonyls such as tricarbonyls might also contribute to this broad band.<sup>66</sup>

**3.1.2. Quantitative analysis – reaction pathways.** Having assigned five key classes of newly formed molecules carrying the carbonyl group, we are now elucidating the underlying formation pathways. For this, we traced the temporal profiles of the deconvoluted bands during the irradiation (Fig. 3) and utilized a set of eleven coupled differential equations to numerically fit these temporal profiles (Fig. 4A).<sup>67</sup> The resulting rate constants are listed in Table 3. Let us consider the pathways that contribute to the formation of acetaldehyde ( $\text{CH}_3\text{CHO}$ ) first. With respect

**Table 2** Deconvoluted peak positions of the carbonyl absorption bands observed in the processed CH<sub>4</sub>-CO, CD<sub>4</sub>-CO, CD<sub>4</sub>-<sup>13</sup>CO, and CH<sub>4</sub>-C<sup>18</sup>O ices

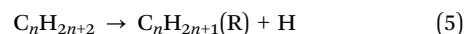
Carrier	CH <sub>4</sub> -CO (cm <sup>-1</sup> )	CD <sub>4</sub> -CO (cm <sup>-1</sup> )	Shift (cm <sup>-1</sup> )	CD <sub>4</sub> - <sup>13</sup> CO (cm <sup>-1</sup> )	Shift (cm <sup>-1</sup> )	CH <sub>4</sub> -C <sup>18</sup> O (cm <sup>-1</sup> )	Shift (cm <sup>-1</sup> )
	1746	1737	11	1691	55	1717	29
	1727	1715	12	1669	58	1694	33
	1717	1695	22	1654	63	1683	34
	1701	1677	24	1639	62	1675	26
	1660	1656	4	1629	31	1656	4
							

to acetaldehyde, the temporal profile and the kinetic fits suggest (pseudo) first order kinetics and the formation of acetaldehyde (CH<sub>3</sub>CHO) within a matrix cage from carbon monoxide-methane *via* recombination of methyl (CH<sub>3</sub>) and formyl (HCO) radicals (*k*<sub>1</sub>). Here, the unimolecular decomposition of methane forms a methyl radical and a suprathreshold hydrogen atom (reaction (1)), which can overcome the barrier to addition to the carbon monoxide molecule leading to the formyl radical (reaction (2)); if both the methyl and formyl radicals have the correct geometrical orientation,<sup>43</sup> they can recombine without barrier to form acetaldehyde (reaction (3)); term symbols are omitted for clarity.

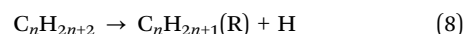
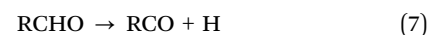


The fits further suggest that higher aldehydes carrying the alkyl group (RCHO) can be synthesized either from the reactants *via* multicenter reactions<sup>37</sup> or by unimolecular decomposition of acetaldehyde *via* hydrogen atom emission leading to the CH<sub>2</sub>CHO radical (reaction (4)); the latter could recombine with an alkyl radical formed *via* radiolysis of the corresponding alkane (reaction (5)) yielding higher aldehydes carrying the

alkyl (reaction(6)). Considering the rate constants, the sequential mechanism involving the recombination of the CH<sub>2</sub>CHO radical with an alkyl radical (*k*<sub>3</sub>) seems to be favorable compared to the multicenter reactions (*k*<sub>2</sub>) by one order of magnitude.



The kinetic scheme further suggests that three reaction pathways can contribute to the formation of saturated ketones with the inherent rate constants *k*<sub>4</sub> to *k*<sub>6</sub>. The first pathway involves a sequential reaction *via* an aldehyde and the inherent formation of an RCO radical intermediate (reaction (7)), which then recombines with an alkyl radical (reaction (8)) forming the ketone (*k*<sub>6</sub>) (reaction (9)).



In the second pathway, acetaldehyde might lose a hydrogen atom from the aldehyde group (reaction (10)), and the resulting

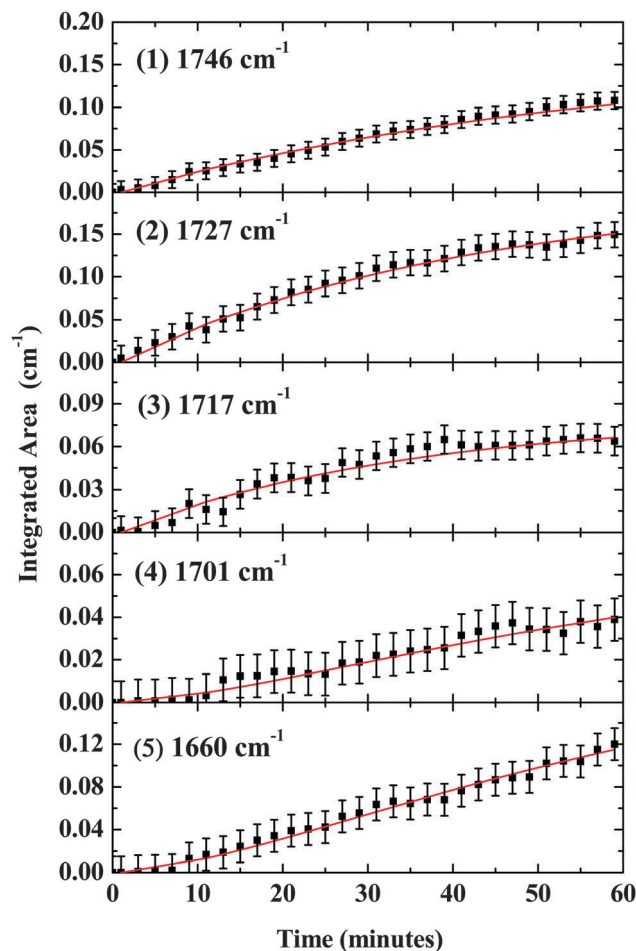
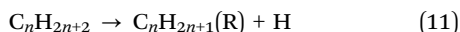


Fig. 3 Fits of the temporal evolution of five classes of molecules: (1) saturated aldehydes (RCHO), (2) acetaldehyde (CH<sub>3</sub>CHO), (3) saturated ketones (RCOR'), (4)  $\alpha,\beta$ -unsaturated aldehydes/ketones, and (5)  $\alpha,\beta,\gamma,\delta$ -unsaturated aldehydes/ketones (5a) and/or  $\alpha,\beta$ -dicarbonyl compounds in keto-enol form (5b).

CH<sub>3</sub>CO radical recombines with an alkyl radical (reaction (11)) forming a saturated methylketone ( $k_5$ ) (reaction (12)).



Alternatively, the fits propose that multicenter reactions from the reactants can lead to ketones ( $k_4$ ). Similar to the formation of the aldehydes, a comparison of the rate constants indicates that multicenter reactions ( $k_4$ ) are less important compared to the sequential formation of ketones *via* aldehydes ( $k_5/k_6$ ). Finally, we propose formation pathways of  $\alpha,\beta$ -unsaturated aldehydes/ketones and also that of  $\alpha,\beta$ -dicarbonyl compounds in keto-enol form and/or  $\alpha,\beta,\gamma,\delta$ -unsaturated aldehydes/ketones.<sup>65</sup> Here, a delayed growth profile for both groups is clearly depicted, strongly indicating that these are higher order products. A detailed analysis of the rate constants (Table 3) indicates that the  $\alpha,\beta$ -unsaturated aldehydes/ketones are predominantly formed *via* radiolysis and

dehydrogenation of the alkyl ketones ( $k_7$ ) (reaction (13)) and only to a smaller extent *via* radiolysis and dehydrogenation of aldehydes ( $k_{11}$ ) (reaction(14)).



Therefore, based on these fits, the absorption feature at 1701 cm<sup>-1</sup> can be likely assigned to  $\alpha,\beta$ -unsaturated ketones. Finally,  $\alpha,\beta$ -dicarbonyl compounds in keto-enol form and/or  $\alpha,\beta,\gamma,\delta$ -unsaturated aldehydes/ketones originated mainly from radiolysis and dehydrogenation of alkyl ketones ( $k_8$ ) and to a minor extent from  $\alpha,\beta$ -unsaturated ketones ( $k_{10}$ ). Therefore, the broad infrared absorption band at 1660 cm<sup>-1</sup> is most likely connected with  $\alpha,\beta,\gamma,\delta$ -unsaturated ketones and to a smaller extent with  $\alpha,\beta$ -dicarbonyl compounds in keto-enol form, which are possibly formed *via* recombination of radiolytically generated RCO radicals (reactions (15) and (16)). Note that to fully reproduce the profile of the 1660 cm<sup>-1</sup> absorption band, it was necessary to include a destruction pathway as well ( $k_{12}$ ).



We can summarize the results of the infrared spectroscopic studies as follows. First, we utilized infrared spectroscopy to identify small, individual molecules with up to two carbon atoms, i.e. simple C2 hydrocarbons such as acetylene (C<sub>2</sub>H<sub>2</sub>), ethylene (C<sub>2</sub>H<sub>4</sub>), and ethane (C<sub>2</sub>H<sub>6</sub>), which have also been observed in the exposure of pure methane ices to ionizing radiation.<sup>47,57</sup> Carbon dioxide (CO<sub>2</sub>) was also observed as a radiation product of radiolyzed neat carbon monoxide ices.<sup>68</sup> We also verified the formation of acetaldehyde (CH<sub>3</sub>CHO) together with the methyl (CH<sub>3</sub>) and formyl (HCO) radicals. Secondly, besides acetaldehyde, we presented compelling evidence based on the vibrational group frequencies for the formation of distinct key classes of organic molecules carrying the carbonyl functional group formed *via* a 'bottom up' synthesis and proposed their formation routes (Fig. 4B): (i) alkyl aldehydes, (ii) alkyl ketones, (iii)  $\alpha,\beta$ -unsaturated ketones and to a smaller extent aldehydes, and (iv)  $\alpha,\beta,\gamma,\delta$ -unsaturated ketones/ $\alpha,\beta$ -dicarbonyl compounds in keto-enol form (Fig. 2); recall that a combination of unsaturated dicarbonyls, and also higher carbonyls such as tricarbonyl molecules might also contribute to this group. Finally, we also provided mechanistical information on the formation routes of these classes. Here, acetaldehyde was identified as the central building block to form saturated aldehydes and ketones; aldehydes have been identified as reaction intermediates to form ketones as well. Both aldehydes and ketones have been traced to lead to the synthesis of  $\alpha,\beta$ -unsaturated ketones and aldehydes; the latter can be radiolyzed, lose hydrogen, and form  $\alpha,\beta,\gamma,\delta$ -unsaturated ketones.  $\alpha,\beta$ -Dicarbonyl compounds are formed from saturated aldehydes and ketone.

**3.1.3. Quantitative analysis – methane and carbon monoxide budget.** Considering the infrared absorption coefficients of  $3.0 \times 10^{-17}$  cm molecule<sup>-1</sup> for the  $\nu_4$  band (1727 cm<sup>-1</sup>) for

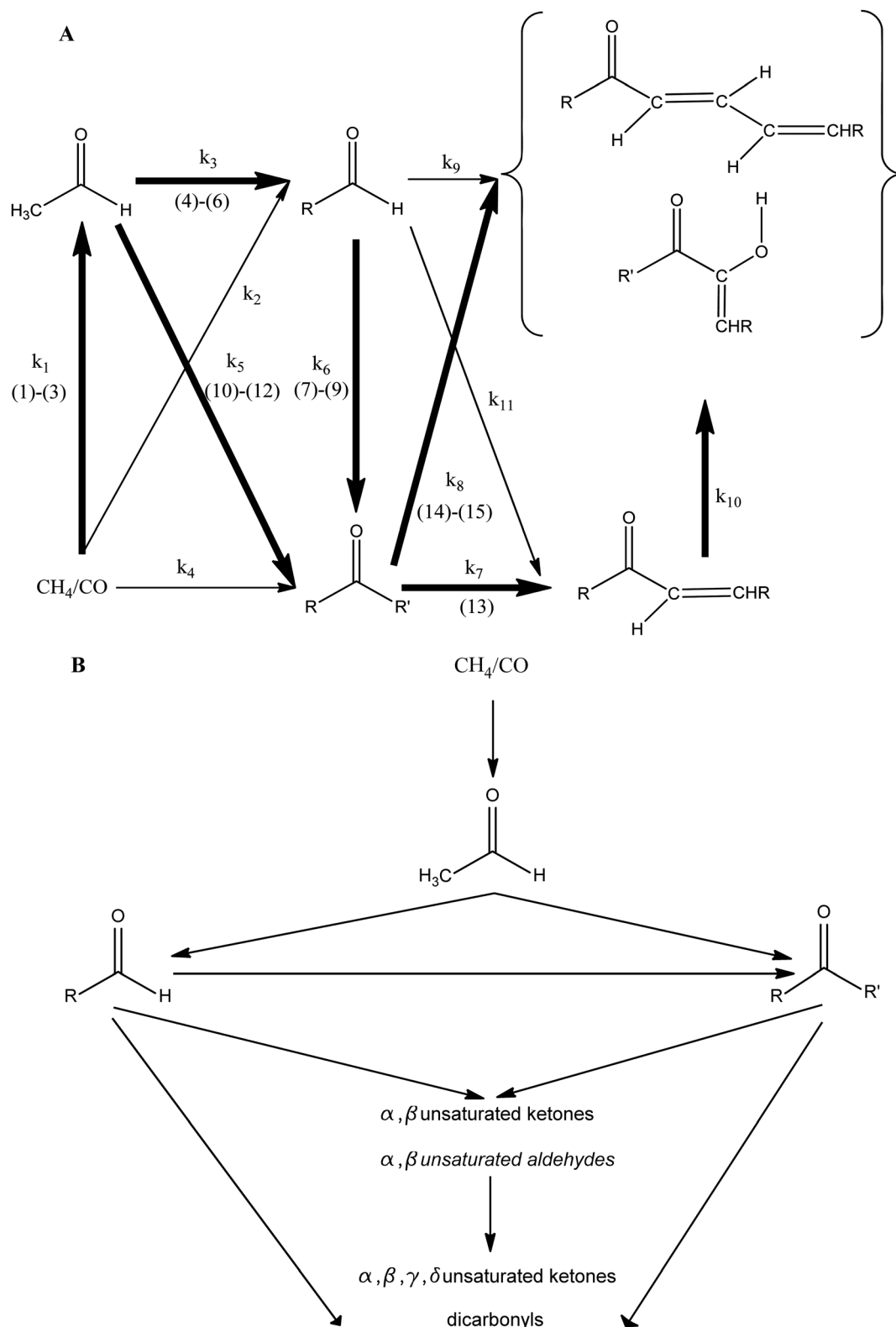


**Fig. 4** (A) Kinetic scheme to fit the temporal evolution of five classes of molecules: (1) saturated aldehydes (RCHO), (2) acetaldehyde (CH<sub>3</sub>CHO), (3) saturated ketones (RCOR'), (4) *α,β*-unsaturated aldehydes/ketones, and (5) *α,β,γ,δ*-unsaturated aldehydes/ketones (5a) and/or *α,β*-dicarbonyl compounds in keto-enol form (5b). Dominating reaction pathways are represented by bold arrows. (B) Bottom-up synthesis of five classes of molecules carrying the carbonyl functional group as derived from the infrared spectroscopic analysis. Species indicated in italics are expected to be minor contributors.

Table 3 Reaction pathways and derived rate constants utilized to fit the temporal evolution of the carbonyl-bearing molecules

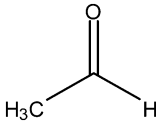
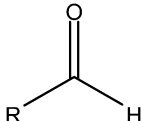
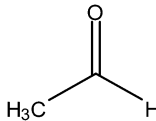
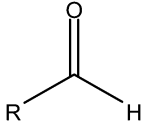
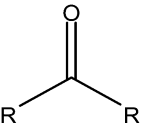
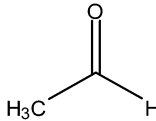
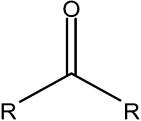
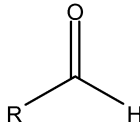
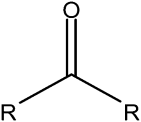
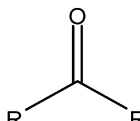
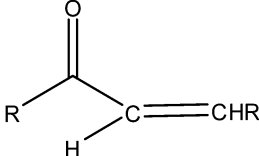
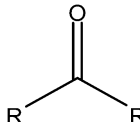
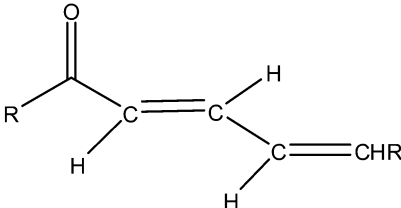
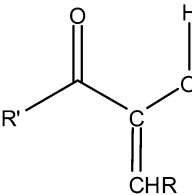
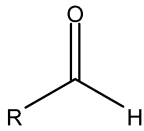
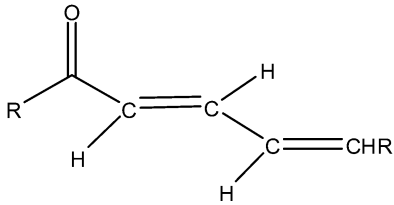
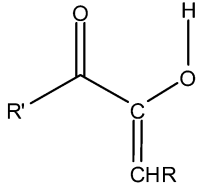
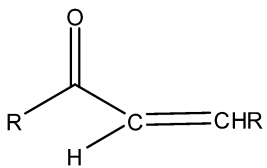
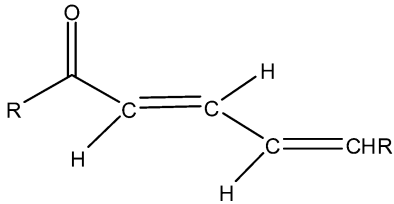
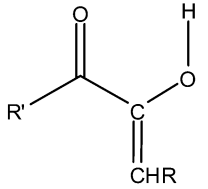
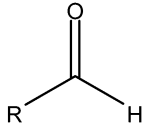
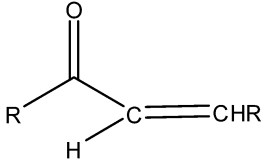
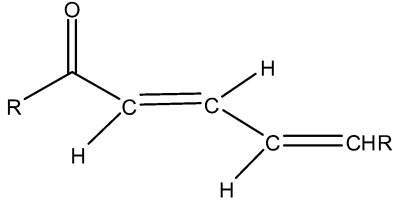
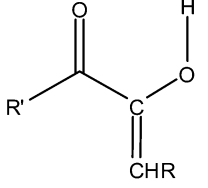
Reactants		Products	Rate constants ( $s^{-1}$ )
$CH_4/CO$	$\longrightarrow$		$k_1 = (1.9 \pm 0.1) \times 10^{-5}$
$CH_4/CO$	$\longrightarrow$		$k_2 = (8.9 \pm 0.8) \times 10^{-6}$
	$\longrightarrow$		$k_3 = (9.8 \pm 0.4) \times 10^{-5}$
$CH_4/CO$	$\longrightarrow$		$k_4 = (9.3 \pm 0.5) \times 10^{-6}$
	$\longrightarrow$		$k_5 = (4.2 \pm 0.4) \times 10^{-4}$
	$\longrightarrow$		$k_6 = (3.4 \pm 0.4) \times 10^{-4}$
	$\longrightarrow$		$k_7 = (5.5 \pm 0.6) \times 10^{-6}$
	$\longrightarrow$		$k_8 = (1.6 \pm 0.2) \times 10^{-3}$
			

Table 3 (continued)

Reactants	Products	Rate constants (s <sup>-1</sup> )
	 	$k_9 = (4.8 \pm 0.5) \times 10^{-7}$
	 	$k_{10} = (5.9 \pm 0.2) \times 10^{-4}$
		$k_{11} = (8.7 \pm 0.8) \times 10^{-7}$
 		$k_{12} = (7.7 \pm 0.5) \times 10^{-4}$

acetaldehyde,  $1.7 \pm 0.2 \times 10^{15}$  molecules  $\text{cm}^{-2}$  were produced during the electron irradiation. This leads to a production rate of  $(7.6 \pm 0.8) \times 10^{-4}$  molecules  $\text{eV}^{-1}$  at 5.5 K and an acetaldehyde yield of  $0.5 \pm 0.1\%$  and  $0.7 \pm 0.1\%$  with respect to methane ( $3.5 \pm 0.4 \times 10^{17}$  molecules  $\text{cm}^{-2}$ ) and carbon

monoxide ( $2.5 \pm 0.1 \times 10^{17}$  molecules  $\text{cm}^{-2}$ ) with their initial column densities presented in parentheses. This production rate is higher than the production rate of acetaldehyde ( $(2.3 \pm 0.5) \times 10^{-4}$  molecules  $\text{eV}^{-1}$ ) previously reported at 10 K.<sup>43</sup> The enhanced production of newly formed molecules with

decreasing temperature represents a well-established trend in the radiation processing of low temperature ices with energetic electrons, if the products are formed *via* the recombination of two radicals within the matrix cage and if these radicals have been produced from closed shell precursors. For instance, Zheng *et al.* demonstrated that upon radiolysis of amorphous water ices, the production rates of molecular hydrogen ( $\text{H}_2$ ) and hydrogen peroxide ( $\text{H}_2\text{O}_2$ ) decrease dramatically from 10 K to 90 K by a factor of about 25 and 50, respectively.<sup>69</sup>

During the irradiation exposure, the number of methane and carbon monoxide molecules dropped from  $3.5 \pm 0.4 \times 10^{17}$  molecules  $\text{cm}^{-2}$  and  $2.5 \pm 0.1 \times 10^{17}$  molecules  $\text{cm}^{-2}$  to  $2.0 \pm 0.2 \times 10^{17}$  molecules  $\text{cm}^{-2}$  and  $2.2 \pm 0.1 \times 10^{17}$  molecules  $\text{cm}^{-2}$ , respectively, thus destroying  $1.5 \pm 0.6 \times 10^{17}$  methane molecules  $\text{cm}^{-2}$  and  $3.0 \pm 2.0 \times 10^{16}$  carbon monoxide molecules  $\text{cm}^{-2}$ . What is the fate of these species? With respect to methane, this species is converted to methyl radicals ( $1.0 \pm 0.1 \times 10^{15}$  molecules  $\text{cm}^{-2}$ ) and the C2 hydrocarbons ethane ( $2.0 \pm 0.2 \times 10^{15}$  molecules  $\text{cm}^{-2}$ ), ethylene ( $1.4 \pm 0.1 \times 10^{15}$  molecules  $\text{cm}^{-2}$ ), and acetylene ( $1.4 \pm 0.1 \times 10^{14}$  molecules  $\text{cm}^{-2}$ ); each of the C2 hydrocarbons requires two methane molecules. Further,  $1.7 \pm 0.2 \times 10^{15}$  molecules  $\text{cm}^{-2}$  are needed to form the acetaldehyde molecules. Therefore,  $9.8 \pm 1.0 \times 10^{15}$  methane molecules were incorporated into methyl, acetaldehyde, and the C2 hydrocarbons accounting for about  $7 \pm 2\%$  of the destroyed methane molecules. With respect to carbon monoxide,  $1.7 \pm 0.2 \times 10^{15}$  molecules  $\text{cm}^{-2}$  are required to account for the acetaldehyde molecules and  $1.0 \pm 0.1 \times 10^{15}$  molecules  $\text{cm}^{-2}$  to produce the formyl radicals. Finally,  $0.9 \pm 0.1 \times 10^{15}$  molecules  $\text{cm}^{-2}$  of carbon dioxide are produced. So in total,  $3.6 \pm 0.4 \times 10^{15}$  carbon monoxide molecules  $\text{cm}^{-2}$  are bound in carbon dioxide, acetaldehyde, and the formyl radical, *i.e.*  $12 \pm 3\%$ . Note that the following infrared absorption coefficients were used:  $3.2 \times 10^{-17}$  cm molecule<sup>-1</sup> ( $3253 \text{ cm}^{-1}$ ;  $\text{C}_2\text{H}_2$ ),  $1.0 \times 10^{-18}$  cm molecule<sup>-1</sup> ( $3093 \text{ cm}^{-1}$ ;  $\text{C}_2\text{H}_4$ ),  $2.7 \times 10^{-18}$  cm molecule<sup>-1</sup> ( $1466 \text{ cm}^{-1}$ ;  $\text{C}_2\text{H}_6$ ),  $1.5 \times 10^{-17}$  cm molecule<sup>-1</sup> ( $1853 \text{ cm}^{-1}$ ;  $\text{HCO}$ ),  $1.4 \times 10^{-17}$  cm molecule<sup>-1</sup> ( $613 \text{ cm}^{-1}$ ;  $\text{CH}_3$ ), and  $7.6 \times 10^{-17}$  cm molecule<sup>-1</sup> ( $2341 \text{ cm}^{-1}$ ;  $\text{CO}_2$ ).<sup>71</sup>

Considering these numbers, it is evident that the majority of methane and carbon monoxide is transformed into higher molecular mass products. Based on the infrared spectra, we provided evidence that besides acetaldehyde, four classes of carbonyl-bearing molecules can be formed. Considering the infrared absorption coefficients of  $1.4 \pm 0.2 \times 10^{-17}$ ,  $1.8 \pm 0.6 \times 10^{-17}$ ,  $1.1 \pm 0.2 \times 10^{-17}$ , and  $1.0 \pm 0.2 \times 10^{-17}$  cm molecule<sup>-1</sup> for the carbonyl stretching frequencies of saturated aldehydes,<sup>62</sup> saturated ketones,  $\alpha,\beta$ -unsaturated aldehydes/ketones and  $\alpha,\beta$ -dicarbonyl compounds in keto-enol form,<sup>70</sup>  $3.3 \pm 0.5 \times 10^{15}$ ,  $1.8 \pm 0.9 \times 10^{15}$ ,  $2.3 \pm 0.4 \times 10^{15}$ , and  $5.7 \pm 1.0 \times 10^{15}$  molecules are formed during the electron irradiation, respectively. Therefore, a total of  $1.9 \pm 0.4 \times 10^{16}$  carbon monoxide molecules have to be consumed to form these compounds. Adding the  $3.6 \pm 0.4 \times 10^{15}$  carbon monoxide molecules  $\text{cm}^{-2}$  bound in carbon dioxide, acetaldehyde, and the formyl radical,  $2.3 \pm 0.4 \times 10^{16}$  carbon monoxide molecules are used up. These data

match well the number of carbon monoxide molecules destroyed ( $3.0 \pm 2.0 \times 10^{16}$  molecules  $\text{cm}^{-2}$ ) calculated from the reduction of the infrared absorption of the  $\nu_1$  fundamental of carbon monoxide. Note that based on the data of the newly formed carbonyl-bearing molecules, we can also estimate how many methane molecules have to be incorporated. Here, each saturated aldehyde requires at least two methane (recall that acetaldehyde has been identified *via* the  $1727 \text{ cm}^{-1}$  absorption and has already been accounted for), each saturated ketone two methane, each  $\alpha,\beta$ -unsaturated aldehyde/ketone at least two (aldehyde) or three (ketone) methane, and  $\alpha,\beta$ -dicarbonyl compounds in keto-enol form<sup>70</sup> at least one (aldehyde) or two (ketone) methane molecules, *i.e.* a total of  $2.8 \pm 1.2 \times 10^{16}$  methane molecules  $\text{cm}^{-2}$ . Adding  $9.8 \pm 1.0 \times 10^{15}$  methane molecules incorporated into methyl, acetaldehyde, and the C2 hydrocarbons, this leads to a total number of methane of  $3.8 \pm 1.3 \times 10^{16}$  molecules  $\text{cm}^{-2}$  accounted for. Considering that  $1.5 \pm 0.6 \times 10^{17}$  methane molecules  $\text{cm}^{-2}$  were destroyed during the irradiation, we have accounted for only  $43 \pm 20\%$  of the methane. Therefore, we have to conclude that the remaining methane molecules were converted into C3 to C5 hydrocarbons (observed *via* QMS/ReTOFMS-PI; Section 3.2) and also into higher mass hydrocarbon side chains of carbonyl-bearing molecules as evident from ReTOF-PI data.

### 3.2. ReTOFMS-PI

Despite impressive FTIR data, with the exception of acetaldehyde, these data alone cannot identify individual molecules carrying the carbonyl functional group simply because the group frequencies, for instance among the saturated aldehydes and ketones, overlap significantly. We thus turned to the complementary, highly sensitive ReTOFMS-PI technique to identify *individual organic molecules carrying the carbonyl group* based on their mass-to-charge ratios, the sublimation temperatures, and how these mass-to-charge ratios shift upon isotope labeling. Fig. 5 depicts the ReTOFMS as a function of temperature during the warm-up phase after irradiating the methane-carbon monoxide ices. The spectra display the intensity of the ion counts of the ionized products subliming into the gas phase at well-defined temperatures. In all systems, molecules with mass up to 200 amu are observable; however, molecular formulas above 116 amu cannot be resolved clearly due to extremely low count rates. By irradiating isotopically labeled ices [ $\text{CD}_4\text{-CO}$ ,  $\text{CD}_4\text{-}^{13}\text{CO}$ ,  $\text{CH}_4\text{-C}^{18}\text{O}$ ], we can assign those mass-to-charge ratios to carbonyl-carrying molecules *via* shift by, for instance, 2 amu (replacing CO by  $\text{C}^{18}\text{O}$ ) or 1 amu (replacing CO by  $^{13}\text{CO}$ ). Further, the isotopically labeled counterparts can be easily identified in all four ices by plotting the sublimation temperatures *versus* the ion counts and verifying that these species hold identical sublimation profiles.<sup>47</sup> This procedure identified eleven classes of molecules subliming into the gas phase.

**3.2.1. Acetaldehyde ( $\text{CH}_3\text{CHO}$ ).** First, we would like to discuss the identification of acetaldehyde. Fig. 6A shows the unique advantages of ReTOFMS coupled to single photon ionization (ReTOFMS-PI) compared to conventional QMS with electron impact ionization of the molecules (QMS-EI). In principle, the signal at  $m/z = 44$  can originate from ionization of carbon

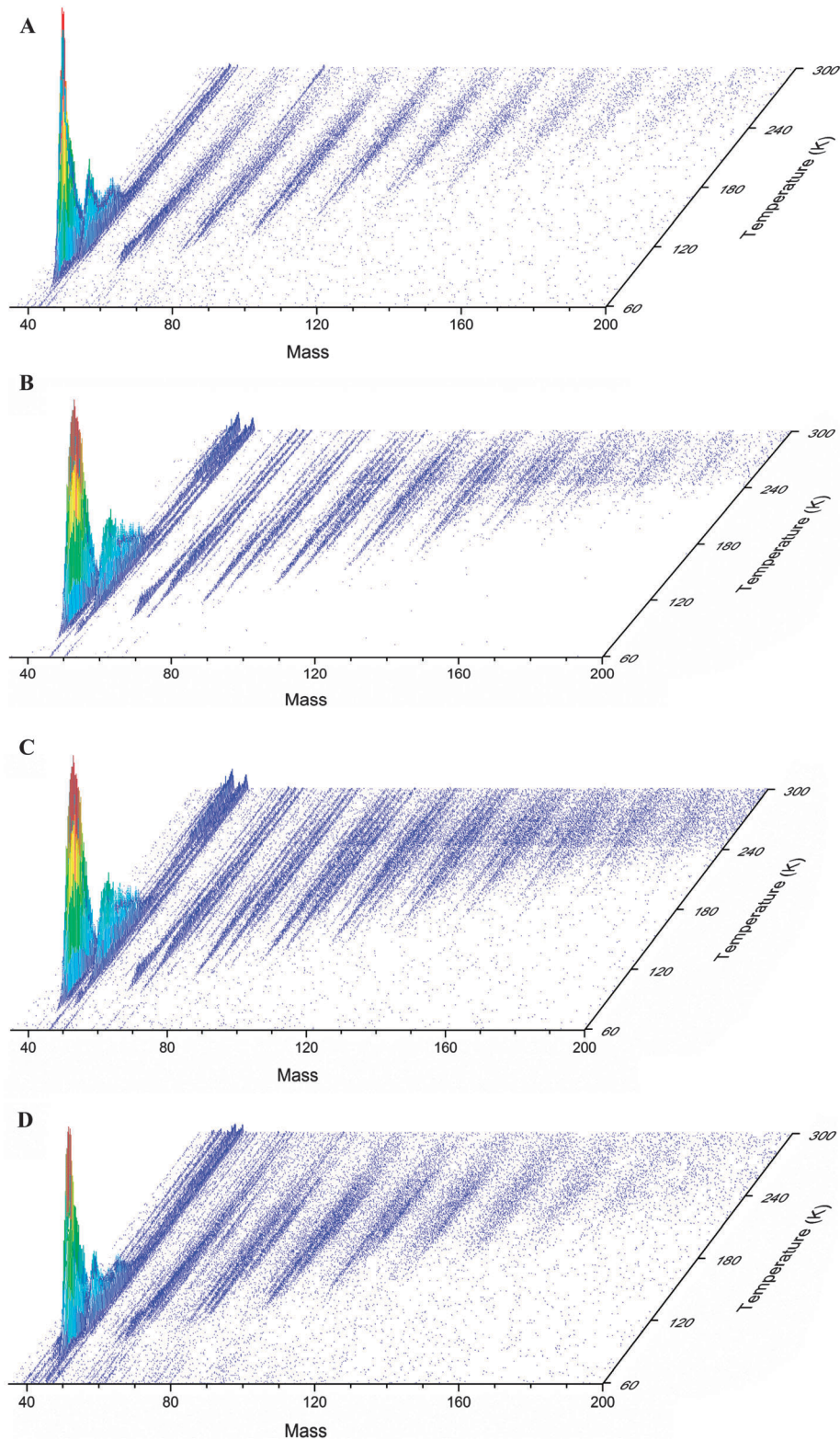


**Fig. 5** (A) ReTOFMS-PI data as a function of temperature of the newly formed products subliming into the gas phase from the radiation processed methane-carbon monoxide ices ( $\text{CH}_4\text{-CO}$ ). (B) ReTOFMS-PI data as a function of temperature of the newly formed products subliming into the gas phase from the radiation processed D4-methane-carbon monoxide ices ( $\text{CD}_4\text{-CO}$ ). (C) ReTOFMS-PI data as a function of temperature of the newly formed products subliming into the gas phase from the radiation processed D4-methane- $^{13}\text{C}$ -carbon monoxide ices ( $\text{CD}_4\text{-}^{13}\text{CO}$ ). (D) ReTOFMS-PI data as a function of temperature of the newly formed products subliming into the gas phase from the radiation processed methane- $^{18}\text{O}$ -carbon monoxide ices ( $\text{CH}_4\text{-C}^{18}\text{O}$ ).

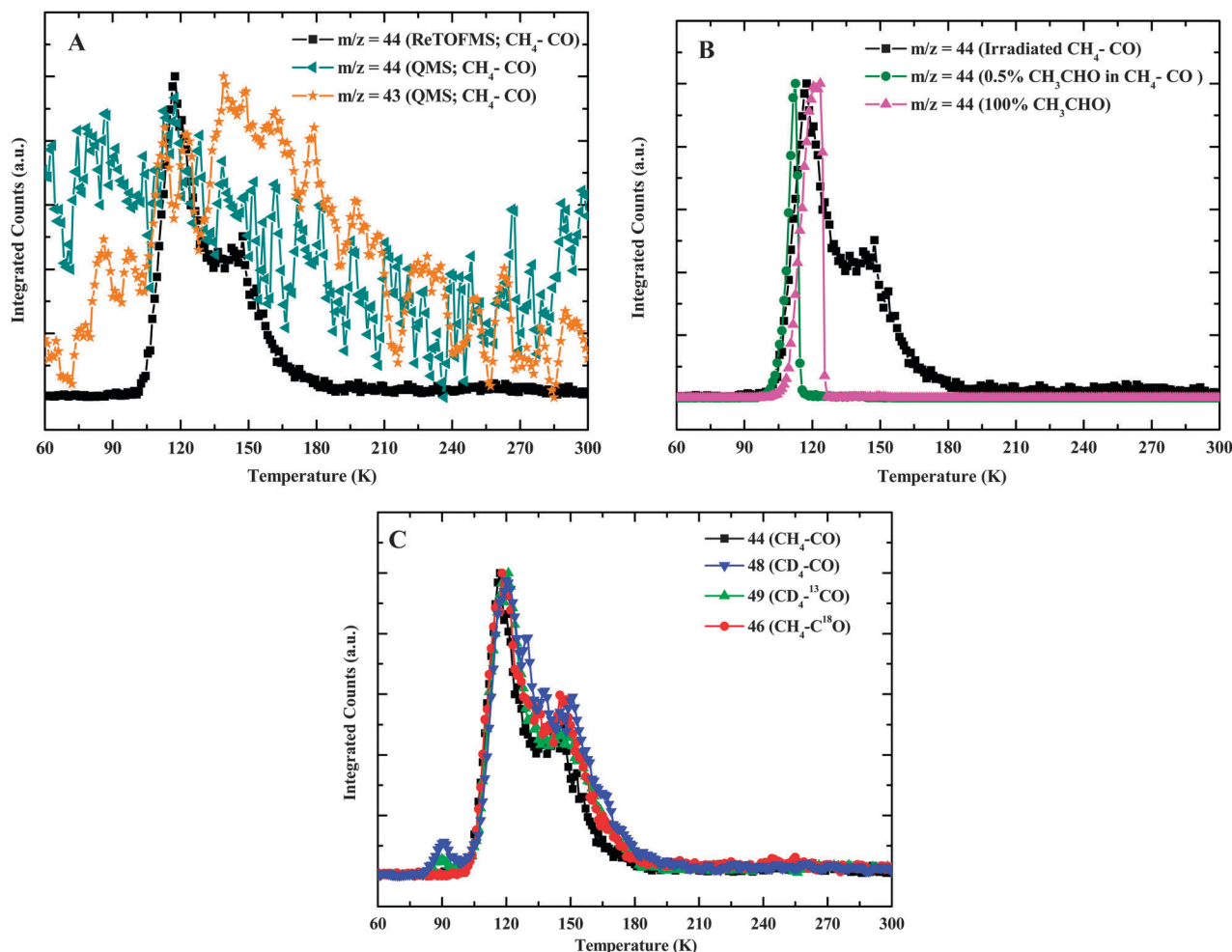


**Fig. 6** (A) Sublimation profiles of the ion counts at  $m/z = 44$  ( $\text{C}_2\text{H}_4\text{O}$ ) recorded with ReTOFMS-PI (black) and QMS-EI (dark-cyan) for the  $\text{CH}_4\text{-CO}$  system. Also overlaid is the ion current of  $m/z = 43$  from the QMS-EI data; this ion can originate from  $\text{C}_3\text{H}_7^+$  as a fragment ion from propane ( $\text{C}_3\text{H}_8$ ) subliming at lower temperatures (70–90 K) as observed in previous irradiation experiments of pure methane ices<sup>47</sup> and from  $\text{CH}_3\text{CO}^+$  as a fragment ion of higher molecular mass methyl ketones (130–300 K) as monitored previously in electron irradiated methane–carbon monoxide ices<sup>47</sup> suggesting sublimation energies up to  $2.5 \text{ kJ mol}^{-1}$  at 300 K. (B) Sublimation profiles of the ion counts at  $m/z = 44$  with ReTOFMS-PI for  $\text{C}_2\text{H}_4\text{O}$  subliming from the irradiated  $\text{CH}_4\text{-CO}$  ice and for acetaldehyde calibration samples containing  $0.5 \pm 0.1\%$  acetaldehyde in  $\text{CH}_4\text{-CO}$  (sample I) and for pure acetaldehyde (sample II). (C) Normalized sublimation profiles of integrated ion counts at  $m/z = 44$  ( $\text{C}_2\text{H}_4\text{O}$ ), 48 ( $\text{C}_2\text{D}_4\text{O}$ ), 49 ( $^{13}\text{C}\text{CD}_4\text{O}$ ) and 46 ( $\text{C}_2\text{H}_4^{18}\text{O}$ ). In the case of  $\text{CD}_4\text{-CO}$  and  $\text{CD}_4\text{-}^{13}\text{CO}$  ices, the distinct peak at around 90 K belongs to  $\text{C}_3\text{D}_6$  ( $m/z = 48$ ) and its  $^{13}\text{C}$  isotopomer ( $m/z = 49$ ), respectively, which have been identified in previous irradiation experiments of pure methane and D4-methane utilizing ReTOFMS-PI;<sup>47</sup> both the propylene (9.73 eV) and the cyclopropane (9.86 eV) isomers can be ionized by the 10.49 eV photon.

dioxide ( $\text{CO}_2$ ), propane ( $\text{C}_3\text{H}_8$ ), and ethylene oxide/acetaldehyde/vinyl alcohol ( $\text{C}_2\text{H}_4\text{O}$ ). In the case of QMS-EI, all possible product molecules can be ionized by the 100 eV electrons giving rise to the dark-cyan graph in Fig. 6A. The signal is dominated by the carbon dioxide background gas essentially prohibiting any assignments. However, ReTOFMS-PI results in a spectrum with an excellent signal-to-noise of about 150 depicting two distinct peaks of the ion current at 117 K and 147 K, respectively. Considering the photon energy of 10.49 eV utilized in the photoionization, contributions from ionized carbon dioxide and propane to  $m/z = 44$  are excluded since their ionization energies of  $10.95 \pm 0.05 \text{ eV}$  and  $13.77 \pm 0.01 \text{ eV}$ <sup>72</sup> are higher than the energy of the 10.49 eV photon. Therefore, the signal at  $m/z = 44$  can only originate from  $\text{C}_2\text{H}_4\text{O}$  isomers. Among the three possible isomers with the molecular formula  $\text{C}_2\text{H}_4\text{O}$  [ethylene oxide ( $\text{c-C}_2\text{H}_4\text{O}$ ),

acetaldehyde ( $\text{CH}_3\text{CHO}$ ), vinyl alcohol ( $\text{CH}_2\text{CHOH}$ )], ethylene oxide has an ionization energy of  $10.56 \pm 0.01 \text{ eV}$ , which is higher than the energy of the photon exploited for the photoionization (10.49 eV); therefore, ethylene oxide does not contribute to any ion signal at  $m/z = 44$ . However, both remaining isomers, acetaldehyde and vinyl alcohol, hold ionization energies of  $10.23 \pm 0.01 \text{ eV}$  and  $9.30 \pm 0.05 \text{ eV}$ , respectively, which are lower than 10.49 eV. Considering that the Re-TOFMS-PI graph at  $m/z = 44$  depicts two pronounced peaks and that two distinct isomers acetaldehyde ( $\text{CH}_3\text{CHO}$ ) and vinyl alcohol ( $\text{CH}_2\text{CHOH}$ ) can be ionized, the data suggest that both isomers are formed in the radiation exposure of methane–carbon monoxide ices in the form of energetic electrons.

In order to assign the ion peaks to acetaldehyde and vinyl alcohol (Fig. 6B), we conducted calibration experiments and

prepared methane-carbon monoxide ices at 5.5 K containing  $0.5 \pm 0.1\%$  acetaldehyde (sample I); recall that based on our FTIR data, the ice after the irradiation contains about  $0.5 \pm 0.1\%$  acetaldehyde together with other product molecules. We also condensed a  $500 \pm 20$  nm thick ice sample of pure acetaldehyde at 5.5 K (sample II). Both ice samples were sublimed under identical conditions as in the real experiments, and the subliming acetaldehyde was photoionized. The resulting graphs of  $m/z = 44$  are plotted in Fig. 6B. Here, the onset of the ion current of  $m/z = 44$  for sample I matched exactly the onset of  $m/z = 44$  for the sublimed irradiated ice at about 100 K rising slightly to 108 K. The ion currents of  $m/z = 44$  peak at 112 K for sample I and at 120 K for sample II; note that the ion current of  $m/z = 44$  for the unknown isomer in the irradiated methane-carbon monoxide ice depicts a maximum of 117 K, which lies between the maxima of the ion count profiles for  $m/z = 44$  for sample I and sample II. Therefore, we can conclude that the acetaldehyde isomer contributes to the ion current at  $m/z = 44$ ; the second peak emerging in the subliming irradiated sample at 147 K cannot be explained with the sublimation of acetaldehyde ( $\text{CH}_3\text{CHO}$ ), but likely originates from the second isomer vinyl alcohol ( $\text{CH}_2\text{CHOH}$ ) interacting *via* stronger hydrogen bonding. Considering the higher polarity of an alcohol compared to an aldehyde, the enhanced sublimation temperature of vinyl alcohol of 147 K compared to acetaldehyde of 117 K is reasonable. Vinyl alcohol, which formally represents the enol form of acetaldehyde, is not stable at room temperature and isomerizes back to acetaldehyde, and hence cannot be purchased to conduct similar calibration experiments as carried out for acetaldehyde. Note that compared to samples I and II, in the irradiated sample, the subliming acetaldehyde depicts a long tail extending up to about 180 K. This pattern is characteristic of higher molecular weight molecules formed in the irradiation process forming a 'cap', thus preventing acetaldehyde from subliming at their nominal sublimation temperature,<sup>58,73</sup> highly polar molecules in particular can interact with acetaldehyde *via* dipole-dipole interactions, hence shifting the sublimation to a broad range of higher temperatures compared to acetaldehyde in methane-carbon monoxide ice (sample I) or pure acetaldehyde (sample II) as reflected in the higher sublimation energies up to  $1.5 \text{ kJ mol}^{-1}$  (180 K) compared to about  $0.9 \text{ kJ mol}^{-1}$  (108 K) for acetaldehyde.

Finally, to verify the identification of acetaldehyde and potentially vinyl alcohol, we probed the sublimation of the isotopically substituted counterparts in the irradiated  $\text{CD}_4\text{-CO}$ ,  $\text{CD}_4\text{-}^{13}\text{CO}$ , and  $\text{CH}_4\text{-C}^{18}\text{O}$  ices and explored their isotope shifts (Fig. 6C). Here, we observed signals at  $m/z = 48$  ( $\text{C}_2\text{D}_4\text{O}$ ) in  $\text{CD}_4\text{-CO}$  ices, at  $m/z = 49$  ( $\text{C}^{13}\text{CD}_4\text{O}$ ) in  $\text{CD}_4\text{-}^{13}\text{CO}$  ices, and at  $m/z = 46$  ( $^{12}\text{C}_2\text{H}_4\text{O}$ ) in  $\text{CH}_4\text{-C}^{18}\text{O}$  ices. The temperature-dependent sublimation profiles are compiled in Fig. 6C. These graphs depict an identical onset of sublimation at  $100 \pm 1$  K of  $m/z = 44$ , 46, 48, and 49. Further, the rise profiles and patterns are identical and also depict two peaks of the ion currents, thus confirming the detection of two distinct products with the molecular formula  $\text{C}_2\text{H}_4\text{O}$  together with their isotopically labeled counterparts: acetaldehyde and vinyl alcohol. Finally, it is important to recall that the formation of acetaldehyde was also confirmed

*via* the detection of  $1727 \text{ cm}^{-1}$  ( $\nu_4$ ),  $1350 \text{ cm}^{-1}$  ( $\nu_7$ ),  $1120 \text{ cm}^{-1}$  ( $\nu_8$ ) and  $1427 \text{ cm}^{-1}$  ( $\nu_{12}$ ) absorption together with its isotopically labeled counterparts. As the temperature increased, the infrared spectra depicted a strong decline of the  $1727 \text{ cm}^{-1}$  absorption, which matches the onset of the ion current profile.

### 3.2.2. Aldehydes and ketones incorporating one carbon monoxide molecule

*Class I.* Besides acetaldehyde ( $\text{CH}_3\text{CHO}$ ;  $\text{C}_2\text{H}_4\text{O}$ ) and vinyl alcohol ( $\text{CH}_2\text{CHOH}$ ;  $\text{C}_2\text{H}_4\text{O}$ ), a detailed analysis of the ReTOFMS-PI data combined with isotopic labeling leads to the identification of a homologous series of fully saturated aldehydes and/or ketones, in which the incorporated carbon monoxide unit stays intact (Table 4):  $\text{C}_2\text{H}_4\text{O}$ ,  $\text{C}_3\text{H}_6\text{O}$ ,  $\text{C}_4\text{H}_8\text{O}$ ,  $\text{C}_5\text{H}_{10}\text{O}$ , and  $\text{C}_6\text{H}_{12}\text{O}$ . The increased molecular weight is also evident from the onset of the sublimation profiles starting at 100 K, 112 K, 119 K, 140 K, and 153 K (Fig. 7A and B). These molecules can be formally derived from their C1 to C5 hydrocarbons [methane ( $\text{CH}_4$ ), ethane ( $\text{C}_2\text{H}_6$ ), propane ( $\text{C}_3\text{H}_8$ ), butane ( $\text{C}_4\text{H}_{10}$ ), and pentane ( $\text{C}_5\text{H}_{12}$ )] and a

Table 4 Molecular formulae of molecules identified in irradiated  $\text{CH}_4\text{-CO}$ ,  $\text{CD}_4\text{-CO}$ ,  $\text{CD}_4\text{-}^{13}\text{CO}$ , and  $\text{CH}_4\text{-C}^{18}\text{O}$  ices utilizing the ReTOFMS together with their sublimation temperatures ( $T_{\text{sub}}$ ) in kelvin (K). Species in italics have been identified tentatively due to the low signal-to-noise

Ices	$\text{CH}_4\text{-CO}$		$\text{CD}_4\text{-CO}$		$\text{CD}_4\text{-}^{13}\text{CO}$		$\text{CH}_4\text{-C}^{18}\text{O}$	
	<i>Formula</i>	$m/z$	$T_{\text{sub}}$	$m/z$	$T_{\text{sub}}$	$m/z$	$T_{\text{sub}}$	$m/z$
$\text{C}_3\text{H}_4$	40	87	44		44	84	40	88
$\text{C}_3\text{H}_6$	42		48	84	48	81	42	81
$\text{C}_2\text{H}_2\text{O}$	42	78	44	78	45	79	44	78
$\text{C}_2\text{H}_4\text{O}$	44	100	48	100	49	99	46	101
<i><math>\text{C}_2\text{H}_6\text{O}</math></i>	46	135	52		53	137	48	
$\text{C}_4\text{H}_6$	54	98	60		60	98	54	98
$\text{C}_4\text{H}_8$	56		64		64	89	56	90
$\text{C}_3\text{H}_4\text{O}$	56	97	60	98	61	97	58	97
<i><math>\text{C}_4\text{H}_{10}</math></i>	58		68	98	68	98	58	
$\text{C}_3\text{H}_6\text{O}$	58	112	64	112	65	111	60	113
$\text{C}_3\text{H}_8\text{O}$	60	134	68	133	69	134	62	134
$\text{C}_5\text{H}_8$	68	108	76	110	76	110	68	108
$\text{C}_4\text{H}_4\text{O}$	68		72	119	73	115	70	
<i><math>\text{C}_5\text{H}_{10}</math></i>	70		80	107	80	106	70	
$\text{C}_4\text{H}_6\text{O}$	70	111	76	112	77	111	72	110
<i><math>\text{C}_5\text{H}_{12}</math></i>	72		84		84		72	106
$\text{C}_4\text{H}_8\text{O}$	72	119	80	118	81	121	74	118
$\text{C}_3\text{H}_4\text{O}_2$	72	116	76		78	118	76	116
$\text{C}_3\text{H}_6\text{O}_2$	74	149	80		82		78	149
$\text{C}_3\text{H}_8\text{O}_2$	76	140	84	140	86	140	80	140
$\text{C}_5\text{H}_6\text{O}$	82	123	88	124	89	123	84	124
$\text{C}_5\text{H}_8\text{O}$	84	130	92		93	127	86	130
<i><math>\text{C}_4\text{H}_4\text{O}_2</math></i>	84		88		90	144	88	
<i><math>\text{C}_5\text{H}_{10}\text{O}</math></i>	86		96	141	97	140	88	139
$\text{C}_4\text{H}_6\text{O}_2$	86	125	92	123	94	125	90	128
$\text{C}_4\text{H}_8\text{O}_2$	88	136	96	137	98	133	92	135
<i><math>\text{C}_4\text{H}_{10}\text{O}_2</math></i>	90		100	152	102		94	148
$\text{C}_6\text{H}_8\text{O}$	96	146	104	142	105	150	98	150
$\text{C}_6\text{H}_{10}\text{O}$	98		108		109	135	100	137
$\text{C}_5\text{H}_6\text{O}_2$	98	145	104	145	106	140	102	143
$\text{C}_6\text{H}_{12}\text{O}$	100	153	112	155	113	153	102	153
$\text{C}_5\text{H}_8\text{O}_2$	100	140	108	140	110	139	104	138
$\text{C}_5\text{H}_6\text{O}_3$	102	155	108		111	149	108	155
$\text{C}_4\text{H}_8\text{O}_3$	104	162	112		115		110	162
$\text{C}_6\text{H}_8\text{O}_2$	112	147	120	146	122	151	116	145
$\text{C}_6\text{H}_{10}\text{O}_2$	114	155	124	155	126	155	118	155
$\text{C}_5\text{H}_6\text{O}_3$	114	155	120	155	123	155	120	155
$\text{C}_5\text{H}_8\text{O}_3$	116	155	124	155	127	155	122	155
<i><math>\text{C}_5\text{H}_{10}\text{O}_3</math></i>	118		128	150	131		124	

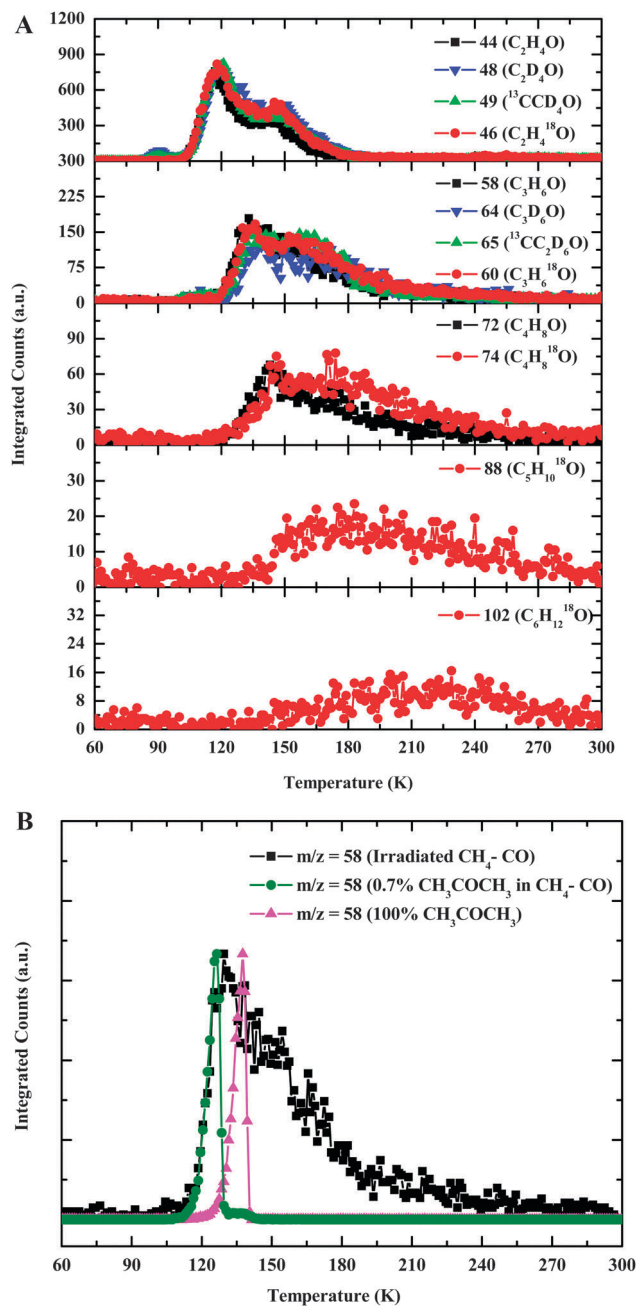


**Fig. 7** (A) Sublimation profiles of saturated aldehydes/ketones. Note that for  $m/z = 44$  ( $C_2H_4O$ ), the double peak hints at the formation of two isomers, acetaldehyde and vinyl alcohol, with distinct polarities. For higher-mass saturated aldehydes/ketones, with the exception of a faint shoulder for  $m/z = 58$  at 158 K, no pronounced peaks emerge proposing that only one isomer is formed or that multiple isomers are synthesized, which have similar sublimation profiles and hence polarities. (B) Sublimation profiles of the ion counts at  $m/z = 58$  with ReTOFMS-PI for  $C_3H_6O$  subliming from the irradiated  $CH_4-CO$  ice and for acetone calibration samples containing  $0.7 \pm 0.1\%$  acetone in  $CH_4-CO$  (sample III) and for pure acetone (sample IV).

single carbon monoxide (CO) building block. Considering potential molecular structures, both acetone ( $CH_3COCH_3$ ; 9.70 eV) and propanal ( $HCOC_2H_5$ ; 9.96 eV) can account for the  $C_3H_6O$  isomer with the ionization energies given in parentheses. To

verify the detection of acetone, we conducted similar calibration experiments as for acetaldehyde (3.2.1). We prepared methane-carbon monoxide ices at 5.5 K containing  $0.7 \pm 0.1\%$  acetone (sample III) as well as pure acetone ices (sample IV) (Fig. 7B). Both ice samples were then sublimed under identical conditions as in the real experiments, and the subliming acetone was photoionized. As shown in Fig. 7B, the onset of the ion current of  $m/z = 58$  for sample III matched exactly the onset of  $m/z = 58$  for the sublimed irradiated ice at 112 K. The ion currents of  $m/z = 58$  peak at 127 K for sample III and at 137 K for sample IV; note that the ion current of  $m/z = 58$  in the real experiment of irradiated methane-carbon monoxide ices depicts a maximum of 130 K, which lies between the maxima of the ion count profiles for  $m/z = 58$  for sample III and sample IV. Therefore, we can conclude that the acetone contributes to the ion current at  $m/z = 58$ . However, the second peak emerging in the subliming irradiated sample at 150 K could have contributions from the keto-enol form of acetone similar to the keto-enol form of acetaldehyde or possibly propanal. With respect to  $C_4H_8O$ , butanal ( $HCOC_3H_7$ ; 9.82 eV), isobutanal ( $HCOC_3H_7$ ; 9.71 eV), and butanone ( $CH_3COC_2H_5$ ; 9.51 eV) can contribute to the ion signal. Note that as the alkyl chain grows, the number of potential structural isomers formed increases significantly from seven to sixteen for  $C_5H_{10}O$  and  $C_6H_{12}O$ , respectively. Recall that the carbonyl functional groups of saturated aldehydes and ketones were also identified *via* FTIR through their 1746 and 1717  $cm^{-1}$  absorptions. Therefore, ReTOFMS-PI data propose that  $C_2H_4O$ ,  $C_3H_6O$ ,  $C_4H_8O$ ,  $C_5H_{10}O$ , and  $C_6H_{12}O$  isomers are the carriers of the 1746 and 1717  $cm^{-1}$  infrared absorptions.

*Class II.* We further identified a homologous series of unsaturated aldehydes and/or ketones (Table 4); similar to class I, the incorporated carbon monoxide molecules stay intact:  $C_3H_4O$ ,  $C_4H_6O$ ,  $C_5H_8O$ , and  $C_6H_{10}O$ . These can be formally derived from the C2 to C5 alkene [ethylene ( $C_2H_4$ ), propylene ( $C_3H_6$ ), butene ( $C_4H_8$ ), and pentene ( $C_5H_{10}$ )] and one carbon monoxide (CO) building block. Similar to the fully saturated aldehydes/ketones, the increase in molecular weight is reflected in a rise of the onset of the sublimation profiles starting at 97 K, 111 K, 130 K, and 135 K (Fig. 8). Here, propenal ( $HCOC_2H_3$ ; 9.8 eV) and cyclopropanone ( $c-C_2H_4CO$ ; 9.1 eV), in which the carbon monoxide molecule is added to the carbon-carbon double bond of ethylene, can contribute to  $m/z = 56$ . Five  $C_4H_6O$  isomers can contribute to the signal at  $m/z = 70$ : *cis/trans*-2-buten-1-al (9.72 eV, 9.73 eV), 2-methyl-propenal (9.86 eV), 3-buten-1-al (9.65 eV), and methylvinylketone (9.65 eV). Note that  $\alpha,\beta$ -unsaturated ketones and aldehydes were predicted to be formed *via* infrared spectroscopy based on the carbonyl group frequency of 1701  $cm^{-1}$ . Hence, ReTOFMS-PI suggests that  $C_3H_4O$ ,  $C_4H_6O$ ,  $C_5H_8O$ , and  $C_6H_{10}O$  isomers might be some of the carriers of the 1701  $cm^{-1}$  infrared absorption.

*Class III.* Our data also suggest the detection of a homologous series of doubly unsaturated aldehydes/ketones (Table 4),  $C_4H_4O$ ,  $C_5H_6O$ , and  $C_6H_8O$ , which can be formally linked to the C3 to C5 [ $C_3H_4$ ,  $C_4H_6$ , and  $C_5H_8$ ] and one carbon monoxide (CO)

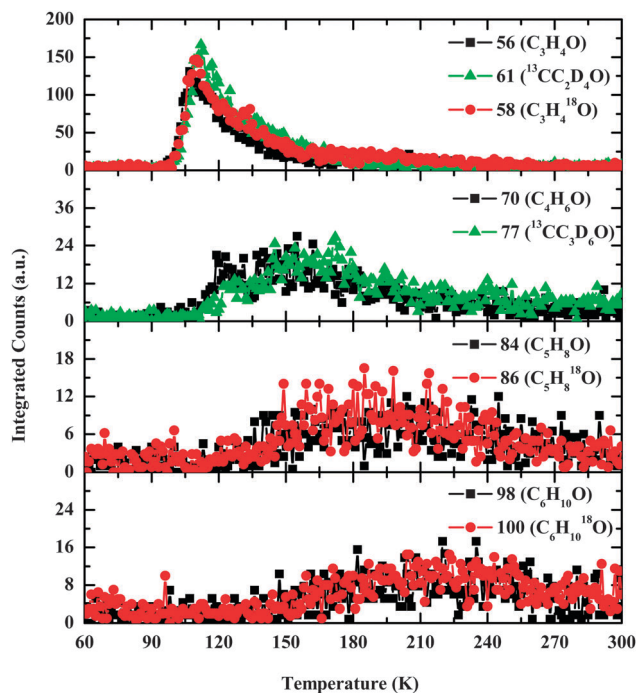


Fig. 8 Sublimation profiles of unsaturated aldehydes/ketones. Note that no pronounced peaks emerge proposing that only one isomer is formed or that multiple isomers are synthesized, which have similar sublimation profiles and hence polarities.

building block. Note that with a rise in molecular mass, the onset of sublimation also shifts to higher temperatures from 119 K *via* 123 K to 146 K for  $C_4H_4O$ ,  $C_5H_6O$ , and  $C_6H_8O$ , respectively (Fig. 9). Considering  $C_4H_4O$ , five isomers might contribute: 2,3-butadien-1-al ( $HCOHCCCH_2$ ) and cyclopropanone-2-ylidene ( $c-C_4H_4O$  as derived from allene) as well as

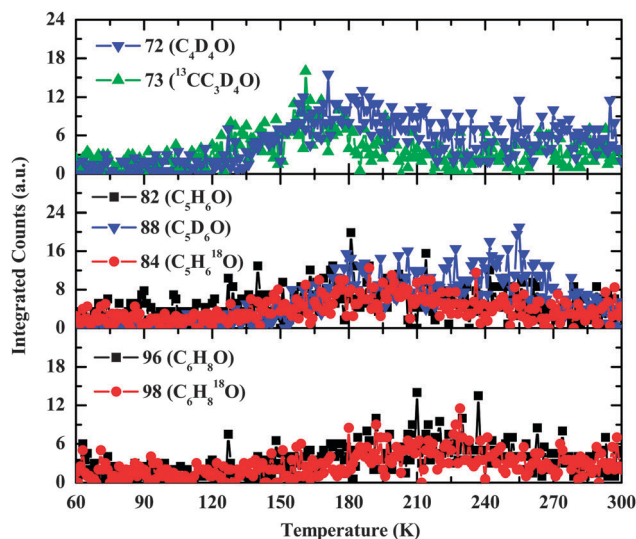


Fig. 9 Sublimation profiles of doubly unsaturated aldehydes/ketones. Note that no pronounced peaks emerge proposing that only one isomer is formed or that multiple isomers are synthesized, which have similar sublimation profiles and hence polarities.

2-butyne-1-al ( $HCOCCCH_3$ ; 10.25 eV), 3-butyne-1-al ( $HCOCH_2CCH$ ), and methylethynylketone ( $CH_3COCCH$ ; 10.25 eV) associated with methylacetylene. Recall that the carbonyl functional group of  $\alpha,\beta,\gamma,\delta$ -unsaturated ketones was also identified *via* FTIR through the  $1660\text{ cm}^{-1}$  absorption. Hence, ReTOFMS-PI proposes that  $C_4H_4O$ ,  $C_5H_6O$ , and  $C_6H_8O$  isomers might be the carriers of the  $1660\text{ cm}^{-1}$  absorption.

It should be noted that the carbonyl-bearing molecules discussed so far can be linked to homologous series of alkanes [C1–C5], alkenes [C2–C5], and diene [C3–C5] building blocks. With the exception of the C1–C3 alkanes and C2 alkene, which have ionization energies higher than the 10.49 eV photon, all other hydrocarbons have been observed *via* ReTOFMS-PI (Fig. 10); as expected, the sublimation temperature rises from the C3 to C5 hydrocarbons from about 81–87 K and 89–98 K to eventually 106–110 K. This trend is consistent with hydrocarbons formed in electron irradiated methane samples at 5.5 K.<sup>47</sup> Methane ( $CH_4$ ), ethane ( $C_2H_6$ ), and ethylene ( $C_2H_4$ ) were monitored *via* infrared spectroscopy (Section 3.1); methane ( $CH_4$ ), ethane ( $C_2H_6$ ), and D8-propane ( $C_3D_8$ ) could also be identified *via* their molecular ions at  $m/z = 16, 30,$  and  $52$  combined with their sublimation temperatures in the residual gas analyzer (QMS); note that  $C_3H_8$  was not observable in the QMS due to interference from the carbon dioxide ( $CO_2$ ) background.

### 3.2.3. Aldehydes and ketones incorporating two and three carbon monoxide molecules

*Class IV.* The species  $C_3H_4O_2$ ,  $C_4H_6O_2$ ,  $C_5H_8O_2$ , and  $C_6H_{10}O_2$  represent the simplest members of molecules having incorporated *two carbon monoxide building blocks*, which can be formally derived from the C1 to C4 hydrocarbons [methane ( $CH_4$ ), ethane ( $C_2H_6$ ), propane ( $C_3H_8$ ), and butane ( $C_4H_{10}$ )] (Fig. 11A). The increased molecular weight is also evident from the onset of the sublimation profiles starting at 116 K, 125 K, 140 K, and 155 K for  $C_3H_4O_2$ ,  $C_4H_6O_2$ ,  $C_5H_8O_2$ , and  $C_6H_{10}O_2$ , respectively. For  $C_3H_4O_2$ , this could account for the isomers propan-1,3-dial ( $HCOCH_2HCO$ ) and propan-2-one-1-al ( $HCOCOCH_3$ ).

*Class V.* A detailed data analysis suggests the formation of the three simplest members of singly unsaturated dicarbonyls  $C_4H_4O_2$ ,  $C_5H_6O_2$ , and  $C_6H_8O_2$ , which are associated with the C2 to C4 alkenes [ethylene ( $C_2H_4$ ), propylene ( $C_3H_6$ ), and butene ( $C_4H_8$ )] plus *two carbon monoxide building blocks* with  $C_4H_4O_2$  identified tentatively (Fig. 11B). Due to the low intensities of the signal, it is difficult to ascertain the exact onset points of sublimation; these are tentatively in the range of 144 to 147 K.

*Class VI.* The  $C_5H_6O_3$  molecule represents the only species that can be decomposed formally into *three carbon monoxide building blocks* plus ethane ( $C_2H_6$ ) (Fig. 11C). Note that the trend of an increasing number of carbonyl groups from one ( $C_3H_6O$ ) *via* two ( $C_4H_6O_2$ ) to three ( $C_5H_6O_3$ ) also results in an increased onset of the sublimation temperatures from 112 K *via* 125 K to 155 K, which is linked to a higher polarity of the molecules as the number of carbonyl groups increases.

*Class VII–IX.* We also derived the synthesis of three product classes holding *one carbonyl plus an alcohol* (class VII; Fig. 11D),

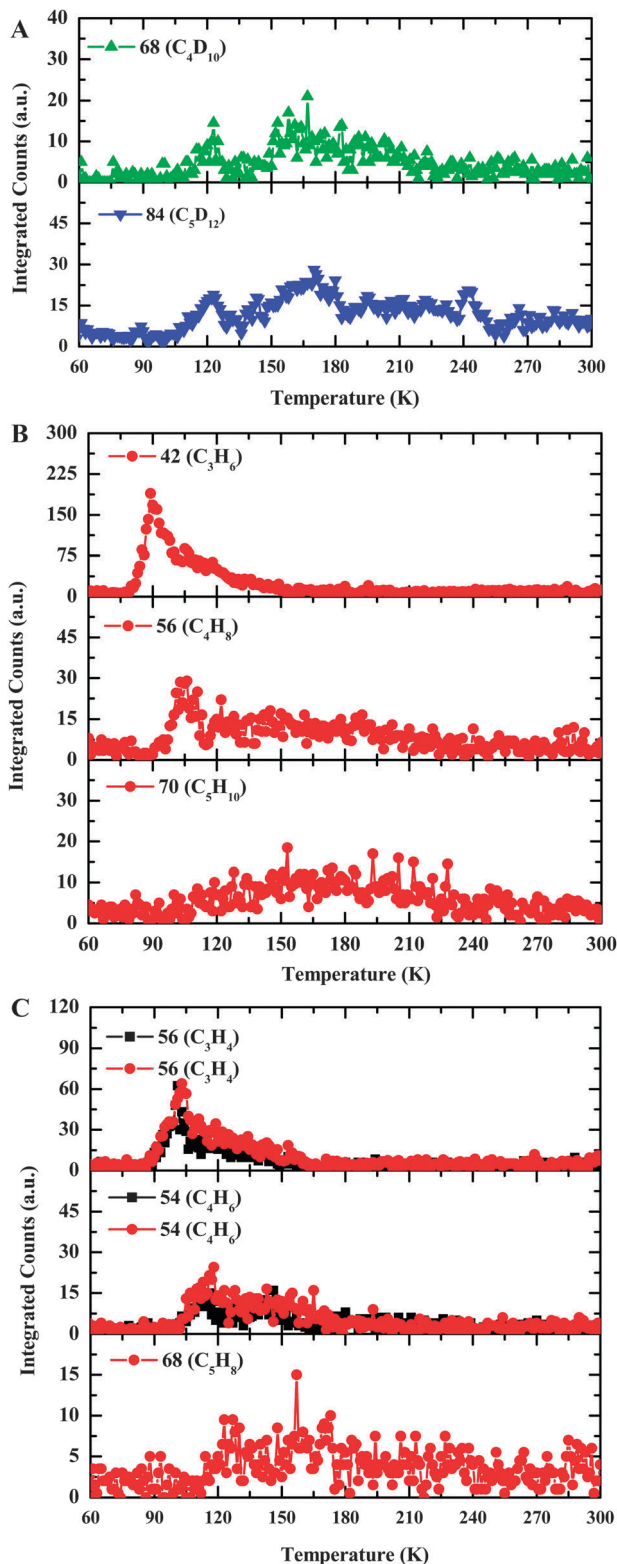


Fig. 10 (A) Sublimation profiles of alkanes identified tentatively. (B) Sublimation profiles of alkenes. Multiple peaks and shoulders such as from C<sub>3</sub>H<sub>6</sub> and C<sub>4</sub>H<sub>8</sub> might hint at the formation of specific isomers. (C) Sublimation profiles of dienes/alkynes.

two carbonyl plus one alcohol (class VIII; Fig. 11E), and one carbonyl plus two alcohol functional groups (class IX; Fig. 11F),

which can be formally classified as (di)hydroxyketones and/or (di)hydroxyaldehydes. These can be formally derived from the C1 and C2 hydrocarbon building blocks [methane (CH<sub>4</sub>), ethane (C<sub>2</sub>H<sub>6</sub>)] holding two carbonyl groups of which one is reduced to an alcohol (C<sub>3</sub>H<sub>6</sub>O<sub>2</sub>, C<sub>4</sub>H<sub>8</sub>O<sub>2</sub>) (class VII), three carbonyl groups of which one is reduced to an alcohol (C<sub>4</sub>H<sub>6</sub>O<sub>3</sub>, C<sub>5</sub>H<sub>8</sub>O<sub>3</sub>) (class VIII), and three carbonyl groups of which two are reduced to an alcohol (C<sub>4</sub>H<sub>8</sub>O<sub>3</sub>, C<sub>5</sub>H<sub>10</sub>O<sub>3</sub>) (class IX), with C<sub>5</sub>H<sub>10</sub>O<sub>3</sub> identified tentatively. Based on the increased polarity of the products, their onset of sublimation increases from class VII to class IX from about 143 ± 7 K *via* 155 ± 1 K to 162 ± 1 K. For the compounds formally derived from the C1 building block methane (CH<sub>4</sub>), the following isomers can account for C<sub>3</sub>H<sub>6</sub>O<sub>2</sub> (class VII): 1-hydroxyacetone (CH<sub>3</sub>COCH<sub>2</sub>OH), 2-hydroxypropanal (CH<sub>3</sub>CHOHCHO), and 3-hydroxypropanal (HOCH<sub>2</sub>CH<sub>2</sub>CHO); the potential structures of more complex isomers formed are too numerous to compile.

**3.2.4. Alcohols.** We also monitored two product classes (class X and XI), which can be derived from incorporated carbon monoxide molecules yielding ketones and/or aldehydes followed by reduction *via* hydrogen addition to form an alcohol (Table 5; Fig. 12). It is important to note that the isotopic pattern verifies that the hydroxyl group originates from hydrogenation of an incorporated carbonyl group, but not from alternative reaction pathways such as insertion of oxygen atoms into carbon–hydrogen bonds or a recombination of an alkyl radical with a hydroxyl (OH) radical.

*Class X.* This class contains the members C<sub>2</sub>H<sub>6</sub>O and C<sub>3</sub>H<sub>8</sub>O, which can be formally derived from C1 and C2 alkanes, methane and ethane, incorporating a carbonyl group followed by reduction to an alcohol (Fig. 12). In the case of C<sub>2</sub>H<sub>6</sub>O, this can account for the formation of ethanol (C<sub>2</sub>H<sub>5</sub>OH; 10.47 eV); dimethylether (CH<sub>3</sub>OCH<sub>3</sub>; 10.03 eV) can be ruled out since this isomer cannot be derived from any aldehyde and/or ketone *via* reduction through hydrogen addition. Therefore, ethanol (C<sub>2</sub>H<sub>5</sub>OH) is formed *via* reduction of acetaldehyde (CH<sub>3</sub>CHO). Considering the C<sub>3</sub>H<sub>8</sub>O isomers, 1-propanol (CH<sub>3</sub>CH<sub>2</sub>OH; 10.22 eV) and 2-propanol (CH<sub>3</sub>CH(OH)CH<sub>3</sub>; 10.12 eV), which can be formed *via* hydrogenation of the carbonyl-bearing molecules acetone (CH<sub>3</sub>COCH<sub>3</sub>) and propanal (HCOC<sub>2</sub>H<sub>5</sub>); note that methylethylether (CH<sub>3</sub>OC<sub>2</sub>H<sub>5</sub>; 9.72 eV) cannot account for the C<sub>3</sub>H<sub>8</sub>O since this isomer does not fulfill the requirement of an incorporated carbon monoxide molecule into a carbonyl functional group, which can then be reduced to the alcohol.

*Class XI.* The C1 and C2 alkanes can also incorporate two carbon monoxide molecules, of which one (class VII) or both (class XI) are reduced *via* hydrogenation to dialcohols (diols) (Fig. 12). For class XI, this leads to the formation of C<sub>3</sub>H<sub>8</sub>O<sub>2</sub> and C<sub>4</sub>H<sub>10</sub>O<sub>2</sub> isomers. For C<sub>3</sub>H<sub>8</sub>O<sub>2</sub>, this can account for the formation of 1,2-propanediol (HOCH<sub>2</sub>CH(OH)CH<sub>3</sub>) and 1,3-propanediol (HOCH<sub>2</sub>CH<sub>2</sub>CH<sub>2</sub>OH). Considering C<sub>4</sub>H<sub>10</sub>O<sub>2</sub>, this can account for the synthesis of dihydroxybutanes and/or dihydroxy isobutanes. It is important to stress that the requirement of reduction of a carbonyl functional group eliminates diols, in which both

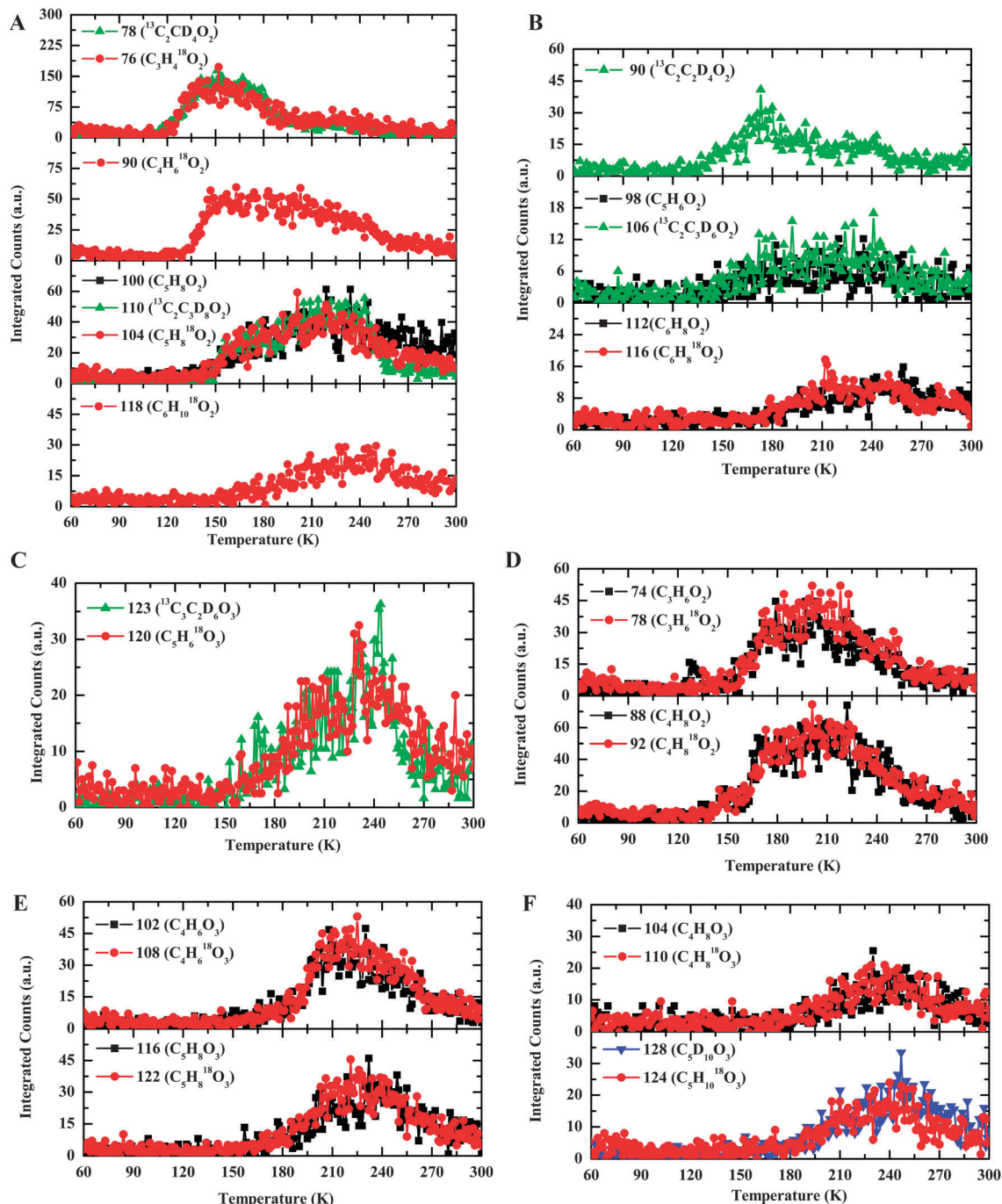


Fig. 11 (A) Sublimation profiles of class IV molecules  $C_3H_4O_2$ ,  $C_4H_6O_2$ ,  $C_5H_8O_2$ , and  $C_6H_{10}O_2$ . (B) Sublimation profiles of class V molecules  $C_4H_4O_2$ ,  $C_5H_6O_2$ , and  $C_6H_8O_2$ . (C) Sublimation profiles of class VI molecule  $C_5H_6O_3$ . (D) Sublimation profiles of class VII molecules  $C_3H_6O_2$  and  $C_4H_8O_2$ . (E) Sublimation profiles of class VIII molecules  $C_4H_6O_3$  and  $C_5H_8O_3$ . (F) Sublimation profiles of class VIII molecules  $C_4H_8O_3$  and  $C_5H_{10}O_3$ .

hydroxyl groups are at the same carbon atom. We also searched for glyoxal ( $HCOCHO$ ; 10.1 eV) and glycolaldehyde ( $HCOCH_2OH$ ; 10.2 eV), but were not successful as the mass shifts of the isotope experiments do not show any similarity in the sublimation profiles. Here, glyoxal could have been formed by recombination of two detected formyl radicals ( $HCO$ ), and glycolaldehyde *via* hydrogenation of one of the carbonyl functional groups in glyoxal. The non-detection of glyoxal proposes that either the

formyl radical concentration is too low so that two formyl radicals can recombine or the formyl radical preferentially recombines with the methyl radical within a matrix cage.

### 3.3. Correlation of infrared and ReTOFMS-PI data

We are linking now the five product classes identified *via* infrared spectroscopy (3.1) with those classified by exploiting ReTOFMS-PI (classes I–XI; 3.2). First, acetaldehyde as well as

**Table 5** Newly formed molecules derived from the C1 (methane) and C2 (ethane) alkanes plus one and two carbon monoxide units, of which one or both are hydrogenated to hydroxyl groups. Species in italics have been identified tentatively due to the low signal-to-noise

Class	Class X	Class VII	Class XI
Hydrocarbon	CO	CO CO	CO CO
CH <sub>4</sub>	↓ +2H <i>C<sub>2</sub>H<sub>6</sub>O</i> ( <i>m/z</i> = 46)	↓ +2H <i>C<sub>3</sub>H<sub>6</sub>O<sub>2</sub></i> ( <i>m/z</i> = 74)	↓ +4H <i>C<sub>3</sub>H<sub>8</sub>O<sub>2</sub></i> ( <i>m/z</i> = 76)
C <sub>2</sub> H <sub>6</sub>	↓ +2H <i>C<sub>3</sub>H<sub>8</sub>O</i> ( <i>m/z</i> = 60)	↓ +2H <i>C<sub>4</sub>H<sub>8</sub>O<sub>2</sub></i> ( <i>m/z</i> = 88)	↓ +4H <i>C<sub>4</sub>H<sub>10</sub>O<sub>2</sub></i> ( <i>m/z</i> = 90)

saturated aldehydes and ketones as identified via infrared spectroscopy can be connected to class I as probed *via* ReTOFMS-PI (Fig. 14). Secondly, the infrared data indicate the formation of  $\alpha,\beta$ -unsaturated ketones and to a smaller extent aldehydes, which can be associated with class II and potentially with class III from the ReTOFMS-PI data. Third,  $\alpha,\beta,\gamma,\delta$ -unsaturated ketones/ $\alpha,\beta$ -dicarbonyls and potentially unsaturated dicarbonyls and also higher carbonyls such as tricarbonyl molecules as assigned *via* infrared spectroscopy are also evident from ReTOFMS-PI *via* classes IV to VI. Note that the infrared data also propose the formation of OH functional groups, which are incorporated into hydrogenated carbonyl groups (class VII–XI).

Finally, it is important to follow the infrared spectra and the development of the absorptions of the carbonyl-bearing molecules as the irradiated samples are warmed up to 300 K (Fig. 13). First, saturated aldehydes (1) are detectable even up to 300 K. The sublimation profile of higher mass saturated aldehydes and ketones such as C<sub>5</sub>H<sub>10</sub>O and C<sub>6</sub>H<sub>12</sub>O (Fig. 7A) as monitored *via* ReTOFMS-PI also exhibits ion counts up to 300 K. Second, infrared intensity of the 1727 cm<sup>-1</sup> carrier assigned as acetaldehyde is observable up to 270 K (2). However, considering the sublimation profile of ReTOFMS-PI the

signal at *m/z* = 44 (Fig. 6A and B) clearly shows that after 180 K, the sublimation of acetaldehyde (*m/z* = 44) is complete. How can this be explained? The remaining intensity at 1727 cm<sup>-1</sup> beyond 180 K likely has contributions from conformers of high mass aldehydes as observed by Coleman *et al.*<sup>63</sup> such as for two conformers of 3-methylbutanal (C<sub>5</sub>H<sub>10</sub>O) *via* infrared absorptions at 1741 and 1729 cm<sup>-1</sup>.<sup>63</sup> As we have seen evidence of higher aldehydes with the molecular formulae of C<sub>5</sub>H<sub>10</sub>O and C<sub>6</sub>H<sub>12</sub>O, higher energy conformers can be populated as the temperature of the samples rises. Finally, infrared absorption bands at 1717 cm<sup>-1</sup> (saturated ketones; (3)), 1701 cm<sup>-1</sup> ( $\alpha,\beta$ -unsaturated aldehydes/ketones; (4)) and 1660 cm<sup>-1</sup> ( $\alpha,\beta,\gamma,\delta$ -unsaturated aldehydes/ketones and/or  $\alpha,\beta$ -dicarbonyl compounds in keto-enol form; (5)) are detectable up to about 230 K. We have seen from the sublimation profiles of class I to VI (Fig. 7–9 and 11) that products with higher masses such as C<sub>6</sub>H<sub>12</sub>O, C<sub>6</sub>H<sub>10</sub>O, and C<sub>6</sub>H<sub>10</sub>O<sub>2</sub> sublime beyond 230 K; the quantity of these molecules is likely below the detection limits of the infrared spectrometer.

## 4. Summary

We investigated the radiation processing of methane–carbon monoxide ices together with their isotopically labeled counterparts with energetic electrons at 5.5 K (Fig. 4B and 14) and probed the newly formed molecules *via* two complementary techniques: FTIR and ReTOFMS-PI. With respect to carbonyl-bearing molecules, the online and *in situ* infrared spectroscopy combined with deconvolution of the ‘carbonyl band’ and kinetically fitting the temporal profiles suggests the ‘bottom up’ formation of acetaldehyde (CH<sub>3</sub>CHO) together with four key classes of carbonyl-bearing molecules (Fig. 4B and 14): (i) alkyl aldehydes, (ii) alkyl ketones, (iii)  $\alpha,\beta$ -unsaturated ketones and to a smaller extent aldehydes, and (iv)  $\alpha,\beta,\gamma,\delta$ -unsaturated ketones/ $\alpha,\beta$ -dicarbonyl compounds in keto-enol form; a combination of

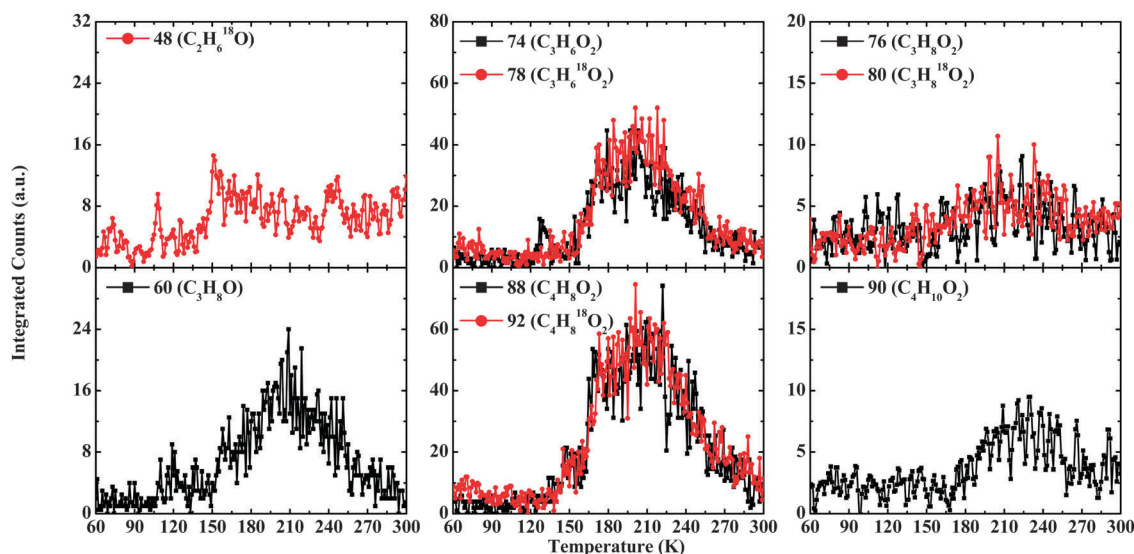


**Fig. 12** Sublimation profiles of class X (C<sub>2</sub>H<sub>6</sub>O and C<sub>3</sub>H<sub>8</sub>O) and class XI (C<sub>3</sub>H<sub>8</sub>O<sub>2</sub> and C<sub>4</sub>H<sub>10</sub>O<sub>2</sub>) molecules (Table 5).

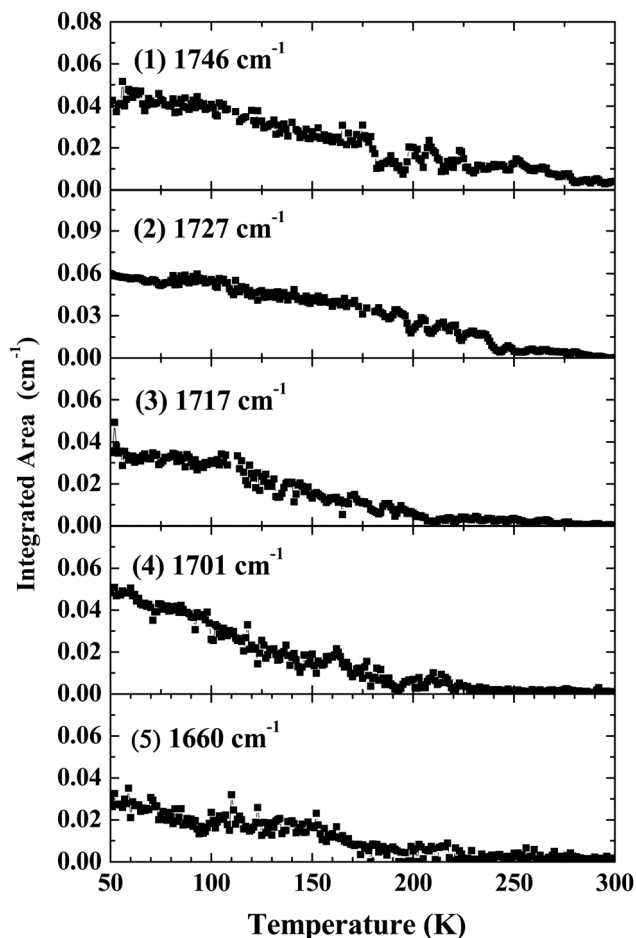


Fig. 13 Temperature programmed desorption profiles of five classes of molecules: (1) saturated aldehydes (RCHO), (2) acetaldehyde ( $\text{CH}_3\text{CHO}$ ), (3) saturated ketones ( $\text{RCOR}'$ ), (4)  $\alpha,\beta$ -unsaturated aldehydes/ketones, and (5)  $\alpha,\beta,\gamma,\delta$ -unsaturated aldehydes/ketones (5a) and/or  $\alpha,\beta$ -dicarbonyl compounds in keto-enol form (5b).

both, *i.e.* unsaturated dicarbonyls, and higher carbonyls such as tricarbonyl molecules might also contribute to this group. Further, we proposed mechanisms for their formation. Acetaldehyde was identified as the key building block of saturated aldehydes and ketones; aldehydes have been identified as reaction intermediates to form ketones as well. Radiolysis of both aldehydes and ketones led to the synthesis of  $\alpha,\beta$ -unsaturated ketones and aldehydes; the latter can be radiolyzed, lose hydrogen, and form  $\alpha,\beta,\gamma,\delta$ -unsaturated ketones.  $\alpha,\beta$ -Dicarbonyl compounds are formed from saturated aldehydes and ketones. With the exception of acetaldehyde, infrared spectroscopy did not identify individual carbonyl-bearing molecules due to their overlapping group frequencies within each class.<sup>66</sup> Therefore, we utilized ReTOFMS-PI coupled with temperature programmed desorption to identify the molecular formulae of *individual organic molecules carrying the carbonyl group* based on their mass-to-charge ratios, the sublimation temperatures, and the correlated mass shift of their respective isotopologues, which can contribute to the product classes observed *via* infrared spectroscopy.

Exploiting ReTOFMS-PI, we identified eleven product classes containing molecules with up to six carbon atoms, which can be formally derived from C1 to C5 hydrocarbons (alkanes, alkenes, dienes) incorporating up to three carbon monoxide building blocks of various degrees of hydrogenation, in which the carbonyl groups stay intact. Fig. 14 links these product classes to those elucidated from infrared spectroscopic studies and fitting of the temporal profiles (Fig. 3 and 4). Selected representatives of important classes are compiled in Fig. 15. These eleven classes are as follows.

#### Class I

This class contains saturated aldehydes and ketones formally derived from their C1 to C5 alkanes [methane ( $\text{CH}_4$ ), ethane ( $\text{C}_2\text{H}_6$ ), propane ( $\text{C}_3\text{H}_8$ ), butane ( $\text{C}_4\text{H}_{10}$ ), and pentane ( $\text{C}_5\text{H}_{12}$ )] and a single carbon monoxide (CO) building block. A detailed analysis of the ReTOFMS-PI data suggests the formation of individual molecules: acetaldehyde ( $\text{CH}_3\text{CHO}$ ;  $\text{C}_2\text{H}_4\text{O}$ ) together with its vinyl alcohol ( $\text{CH}_2\text{CHOH}$ ;  $\text{C}_2\text{H}_4\text{O}$ ) isomer, acetone ( $\text{CH}_3\text{COCH}_3$ ) and possibly propanal ( $\text{HCOC}_2\text{H}_5$ ), and butanal ( $\text{HCOC}_3\text{H}_7$ ), isobutanal ( $\text{HCOC}_3\text{H}_7$ ), and/or butanone ( $\text{CH}_3\text{COC}_2\text{H}_5$ ). These molecules as observed upon their sublimation can be linked to the 1746 and 1717  $\text{cm}^{-1}$  group frequencies for saturated aldehydes and ketones, respectively. Reaction mechanisms linking acetaldehyde ( $\text{CH}_3\text{CHO}$ ) to acetone ( $\text{CH}_3\text{COCH}_3$ ), propanal ( $\text{HCOC}_2\text{H}_5$ ), and higher aldehydes/ketones are compiled in Fig. 4B.

#### Class II

This includes unsaturated aldehydes and/or ketones formally derived from their C1 to C5 alkenes [ethylene ( $\text{C}_2\text{H}_4$ ), propylene ( $\text{C}_3\text{H}_6$ ), butene ( $\text{C}_4\text{H}_8$ ), and pentene ( $\text{C}_5\text{H}_{10}$ )] and a single carbon monoxide (CO) building block. Here, propenal ( $\text{HCOC}_2\text{H}_3$ ) and cyclopropanone ( $c\text{-C}_2\text{H}_4\text{CO}$ ) can contribute to the  $\text{C}_3\text{H}_4\text{O}$  isomers. Methylvinylketone ( $\text{CH}_3\text{COC}_2\text{H}_3$ ) might add to the  $\text{C}_4\text{H}_6\text{O}$  isomers. Here,  $\alpha,\beta$ -unsaturated ketones and aldehydes were predicted to be synthesized *via* infrared spectroscopy based on the carbonyl group frequencies of 1701  $\text{cm}^{-1}$ . These class II molecules can be linked to their class I parents by oxidation (dehydrogenation) of the alkyl side chain.

#### Class III

This comprises doubly unsaturated aldehydes/ketones formally derived from their C3 to C5 dienes/alkynes [ $\text{C}_3\text{H}_4$ ,  $\text{C}_4\text{H}_6$ , and  $\text{C}_5\text{H}_8$ ] and one carbon monoxide (CO) building block. Methyl-ethynylketone might be the simplest isomer contributing to  $\text{C}_4\text{H}_4\text{O}$ . The carbonyl functional group of  $\alpha,\beta,\gamma,\delta$ -unsaturated ketones was also identified *via* FTIR through the 1660  $\text{cm}^{-1}$  absorption. Class III molecules can be linked to their class II parents by oxidation (dehydrogenation) of the alkenyl side chain.

#### Class IV

This class includes saturated dialdehydes and diketones formally derived from the C1 to C4 hydrocarbons [methane ( $\text{CH}_4$ ), ethane ( $\text{C}_2\text{H}_6$ ), propane ( $\text{C}_3\text{H}_8$ ), and butane ( $\text{C}_4\text{H}_{10}$ )] and two carbon monoxide (CO) building blocks. For the simplest  $\text{C}_3\text{H}_4\text{O}_2$  formula, only two isomers can contribute: propan-1,3-dial ( $\text{HCOCH}_2\text{HCO}$ )

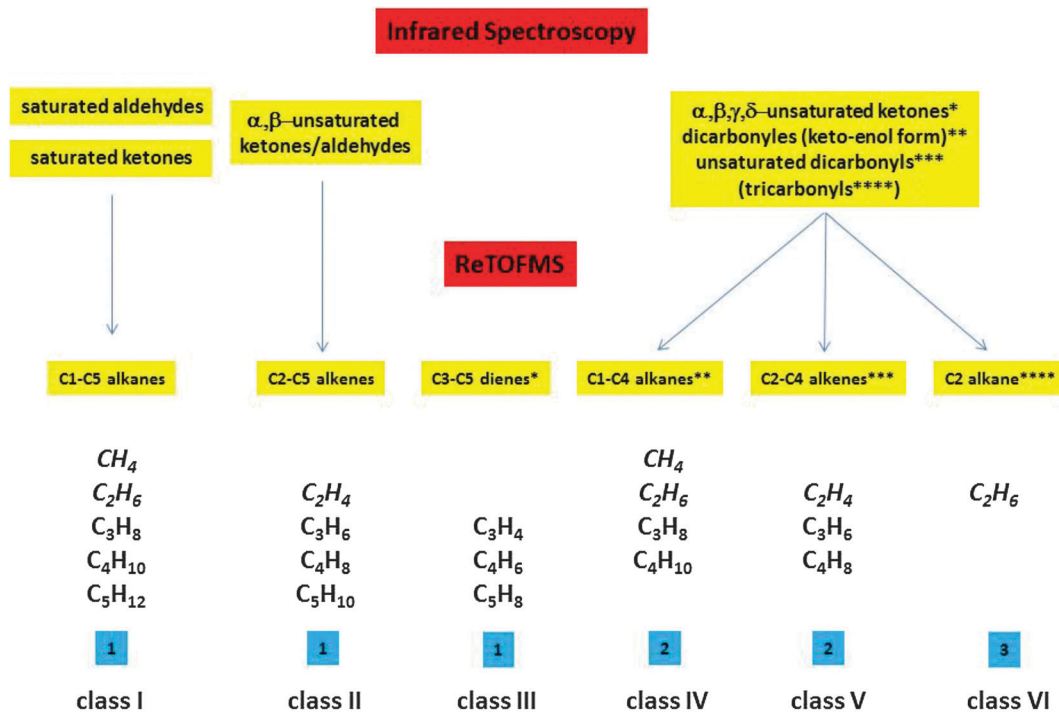


Fig. 14 Summary of product classes detected *via* infrared (top) and ReTOFMS-PI (bottom) analysis of the irradiated methane-carbon monoxide ices. The numbers of incorporated carbon monoxide molecules are defined in the blue boxes. The C1–C5 hydrocarbon building blocks are also defined for each class.

and propan-2-one-1-al (HCOCOCH<sub>3</sub>). Note that dicarbonyls in the enol form were also proposed to be the carrier of the 1660 cm<sup>-1</sup> absorption. Reaction mechanisms linking these diones to acetaldehyde (CH<sub>3</sub>CHO) (class I) are compiled in Fig. 4B.

#### Class V

This includes unsaturated aldehydes/ketones formally derived from the C2 to C4 alkenes [ethylene (C<sub>2</sub>H<sub>4</sub>), propylene (C<sub>3</sub>H<sub>6</sub>), and butene (C<sub>4</sub>H<sub>8</sub>)] and two carbon monoxide (CO) building blocks. Recall that  $\alpha,\beta$ -unsaturated dicarbonyls could also contribute to the 1660 cm<sup>-1</sup> absorption. These class V molecules can be linked to class II precursors as compiled in Fig. 4B.

#### Class VI

This class comprises saturated aldehydes and ketones formally derived from the C2 alkane [ethane (C<sub>2</sub>H<sub>6</sub>)] and three carbon monoxide (CO) building blocks. Tricarbonyls might also absorb in the 1660 cm<sup>-1</sup> region. These class V molecules might be connected to class III *via* radiolysis similar to the formation of diketones from ketones/aldehydes.

#### Class VII–IX

Class VII–IX include (di)hydroxyaldehydes/(di)hydroxyketones with one carbonyl plus an alcohol (class VII), two carbonyl plus one alcohol (class VIII), and one carbonyl plus two alcohol functional groups (class IX) formally derived from the C1 and C2 alkanes [methane (CH<sub>4</sub>), ethane (C<sub>2</sub>H<sub>6</sub>)] holding two carbonyl groups of which one is reduced to an alcohol (class VII), three carbonyl groups of which one is reduced to

an alcohol (class VIII), and three carbonyl groups of which two are reduced to an alcohol (class IX). For the compounds derived from the C1 building block methane (CH<sub>4</sub>), 1-hydroxyacetone (CH<sub>3</sub>COCH<sub>2</sub>OH), 2-hydroxypropanal (CH<sub>3</sub>CHOHCHO), and 3-hydroxypropanal (HOCH<sub>2</sub>CH<sub>2</sub>CHO) can account for the C<sub>3</sub>H<sub>6</sub>O<sub>2</sub> isomer (class VII). This class, for instance, can be derived from class IV *via* hydrogenation of one of the carbonyl groups.

#### Class X

This includes alcohols formally derived from their C1 to C2 alkanes [methane (CH<sub>4</sub>), ethane (C<sub>2</sub>H<sub>6</sub>)] incorporating a carbonyl group, which is reduced to an alcohol. The data account for the formation of ethanol (C<sub>2</sub>H<sub>5</sub>OH) and 1-propanol (CH<sub>3</sub>CH<sub>2</sub>CH<sub>2</sub>OH) and/or 2-propanol (CH<sub>3</sub>CH(OH)CH<sub>3</sub>), which can be formed *via* hydrogenation of the class I molecules acetone (CH<sub>3</sub>COCH<sub>3</sub>) and propanal (HCOC<sub>2</sub>H<sub>5</sub>).

#### Class XI

This includes diols formally derived from their C1 to C2 alkanes [methane (CH<sub>4</sub>), ethane (C<sub>2</sub>H<sub>6</sub>)] incorporating two carbonyl groups, which are both reduced to a diol as derived *via* hydrogenation of class VII–IX molecules.

Utilizing the experimental techniques described above, we finally made crucial progress toward a detailed understanding of which complex organic molecules – those holding carbonyl functional groups in particular – are formed in the radiation-induced processing of simple binary ices of methane and carbon monoxide *in bulk ices*. By arranging the newly formed molecules/isomers into distinct classes, we were also able to

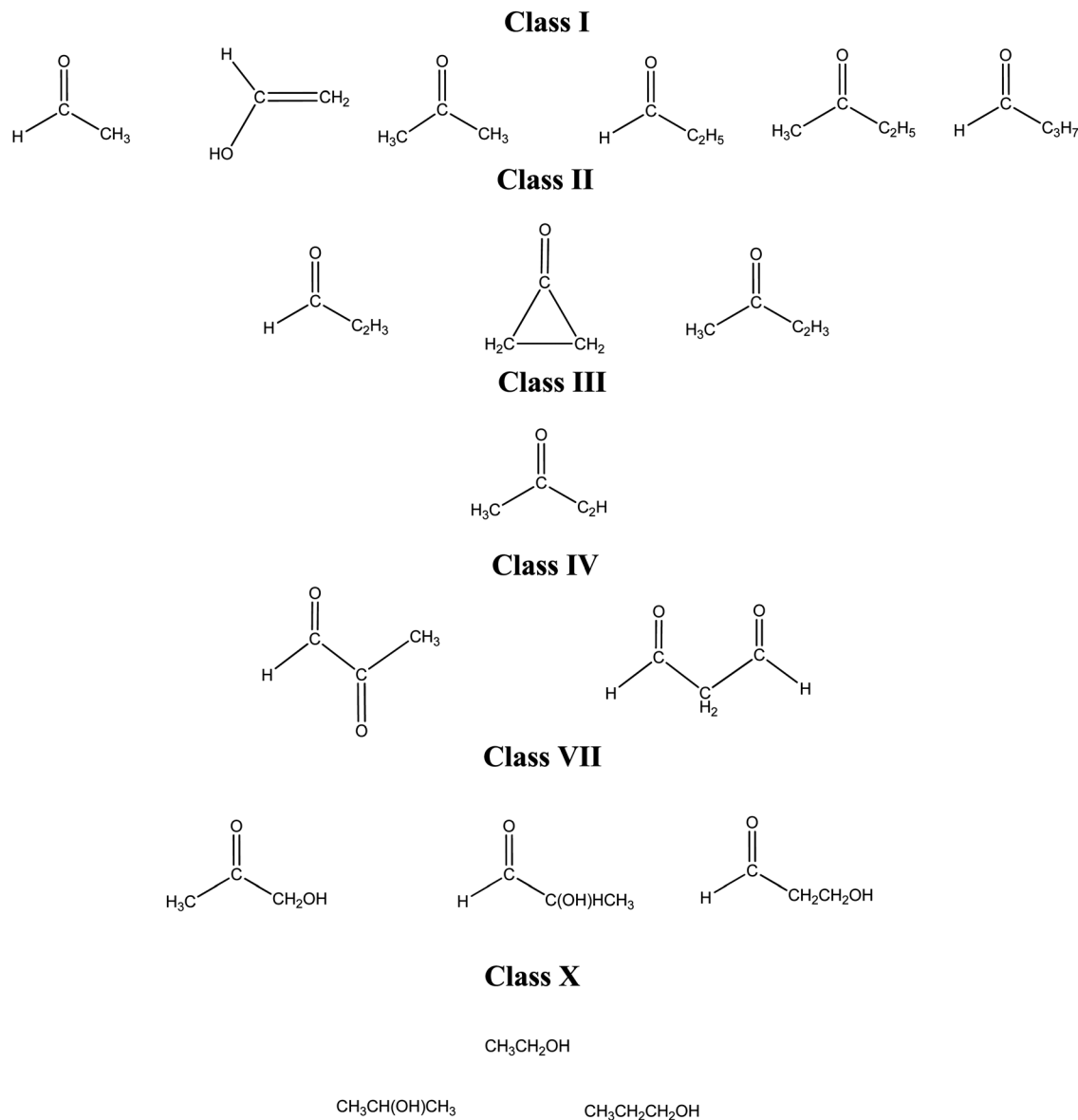


Fig. 15 Chemical structures of selected isomers derived from C1 to C3 hydrocarbons, which can account for the molecules observed via ReTOFMS-PI.

derive possible formation pathways linking the eleven classes among each other *via*, for example, reduction (hydrogenation), radiolysis of the aldehydes/ketones to form dicarbonyls, and radiolysis leading to unsaturated counterparts. Finally, we also identified – besides the molecular formulae – individual molecules such as acetaldehyde, vinylalcohol, acetone, and ethanol, and proposed carriers of distinct representatives of selected classes as well. Here, future experiments will exploit a newly built pulsed coherent VUV light source (4 eV to 13 eV) utilizing resonance-enhanced nonlinear four wave mixing to photo-ionize the subliming molecules at different wavelengths. This will aid in the identification of additional, specific isomers based upon their distinctive ionization energies to eventually provide a comprehensive inventory of the molecules that can be formed on icy interstellar grains upon radiation. Further, we are planning to conduct additional calibration experiments as

shown here for acetaldehyde and acetone in an attempt to elucidate the nature of distinct molecules based on their sublimation temperatures and mass-to-charge ratios.

So far, only 15 organic molecules carrying the carbonyl functional group have been detected in the interstellar medium (Fig. 16) predominantly in hot cores such as Sgr(B2). Our studies provide solid evidence that among these observed molecules, acetaldehyde (CH<sub>3</sub>CHO) and acetone (CH<sub>3</sub>COCH<sub>3</sub>) and possibly propanal (HCOC<sub>2</sub>H<sub>5</sub>) together with propenal (HCOC<sub>2</sub>H<sub>5</sub>) – subject to verification of the sublimation temperatures and ionization energies – can be formed upon interaction of methane-carbon monoxide ices with energetic electrons. Previous laboratory experiments in our group also provided compelling evidence that the propynal (HCCCHO)–cyclopropanone (c-C<sub>3</sub>H<sub>2</sub>O) can both be formed from acetylene (C<sub>2</sub>H<sub>2</sub>) and carbon monoxide at 10 K upon radiolysis.<sup>74</sup> Likewise, formic acid (HCOOH) and

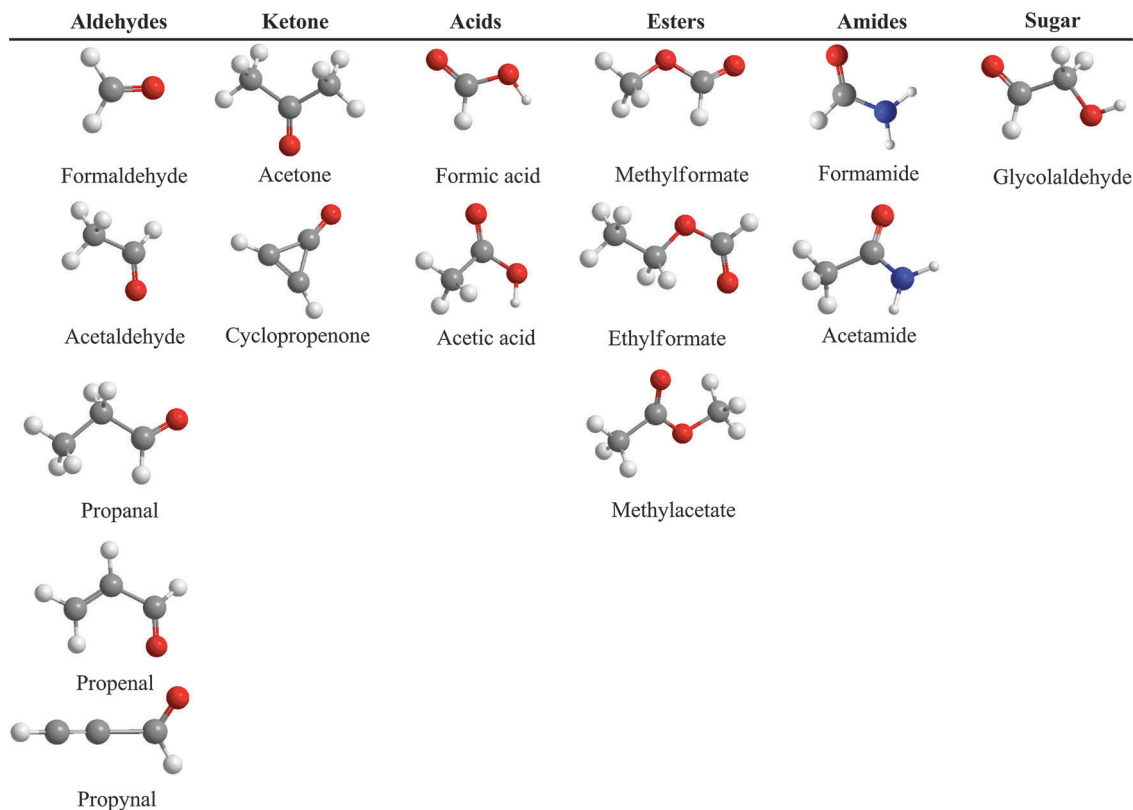


Fig. 16 Organic molecules carrying the carbonyl group detected in the interstellar medium (ISM).

acetic acid ( $\text{CH}_3\text{COOH}$ ) can be synthesized in water ( $\text{H}_2\text{O}$ )–carbon monoxide ( $\text{CO}$ )<sup>75</sup> and methane ( $\text{CH}_3$ )–carbon dioxide ices ( $\text{CO}_2$ ).<sup>5</sup> The methylformate ( $\text{CH}_3\text{COOCH}_3$ ) and glycolaldehyde ( $\text{HCOCH}_2\text{OH}$ ) isomers were found to be both synthesized in methanol ( $\text{CH}_3\text{OH}$ )–carbon monoxide ( $\text{CO}$ ) ices upon electron exposure at 10 K;<sup>6</sup> note that glycolaldehyde ( $\text{HCOCH}_2\text{OH}$ ) was also formed in pure methanol ( $\text{CH}_3\text{OH}$ ) upon radiolysis with energetic electrons at 10 K.<sup>76</sup> Finally, Jones al. showed that formamide ( $\text{HCONH}_2$ ) – the simplest molecule carrying a peptide bond – is created by electron exposure of carbon monoxide ( $\text{CO}$ )–ammonia ( $\text{NH}_3$ ) ices.<sup>77</sup> Based on the infrared features emerging during the irradiation of the low temperature ices, these molecules are formed inside the bulk of low temperature (10 K) ices holding thicknesses of a few 100 nm upon exposure to energetic electrons involving non-equilibrium (non-thermal, suprathreshold) chemistry. However, additional reaction pathways can be triggered by heating up the irradiated samples, *i.e.* simulating the transition of the molecular cloud to star forming regions. Here, the low temperature can still store reactive radicals, which might recombine upon warming up. Therefore, our current study and the compilation of newly formed molecules (Fig. 14 and 15) should guide searches of these molecules in the interstellar medium. Since the actual synthesis occurs in cold molecular clouds such as TMC-1 inside the 10 K ices, subsequent sublimation processes – similar to our warm-up phase – has to transform these molecules from the ices into the gas phase. This can be achieved once the molecular cloud transforms to star forming regions in which

the elevated temperatures of up to 250 K facilitate the release of the newly formed molecules from the ices into the gas phase. Therefore, guided by laboratory studies as presented here, prospective searches with ALMA toward SgrB2, for instance, are expected to identify numerous, hitherto unobserved molecules in the interstellar medium which carry carbonyl functional groups. Previous searches of hydroxyketones such as 1,3-dihydroxyacetone have remained inconclusive.<sup>78</sup> However, our studies propose that  $\text{C}_3\text{H}_6\text{O}_2$  molecules – most likely hydroxyacetone – should be formed upon interaction of ionizing radiation with methane–carbon monoxide ices.

## Acknowledgements

The authors would like to thank the W.M. Keck Foundation, the University of Hawaii and the NASA Exobiology Program NNX13AH62G.

## References

- 1 A. I. Vasyunin and E. Herbst, *Astrophys. J.*, 2013, **769**, 34.
- 2 Å. Hjalmarson, P. Bergman, A. Nummelin, Proc. 1st European Workshop on Exo-/astro-biology (ESA SP-496), Noordwijk, ESA, 2001.
- 3 D. T. Halfen, V. Ilyushin and L. M. Ziurys, *Astrophys. J.*, 2011, **743**, 60.

- 4 C. J. Bennett, S.-H. Chen, B.-J. Sun, A. H. H. Chang and R. I. Kaiser, *Astrophys. J.*, 2007, **660**, 1588–1608.
- 5 C. J. Bennett and R. I. Kaiser, *Astrophys. J.*, 2007, **660**, 1289–1295.
- 6 C. J. Bennett and R. I. Kaiser, *Astrophys. J.*, 2007, **661**, 899–909.
- 7 A. F. Jalbout, *Origins Life Evol. Biospheres*, 2008, **38**, 489–497.
- 8 Y. J. Kuan, S. B. Charnley, H. C. Huang, W. L. Tseng and Z. Kisiel, *Astrophys. J.*, 2003, **593**, 848–867.
- 9 C. A. Gottlieb, *Molecules in the galactic environment*, Wiley, New York, 1973.
- 10 S. G. Brunken, C. A. Gottlieb, M. C. McCarthy and P. Thaddeus, *Astrophys. J.*, 2007, **664**, L43–L46.
- 11 M. C. McCarthy, C. A. Gottlieb, H. Gupta and P. Thaddeus, *Astrophys. J.*, 2006, **652**, L141–L144.
- 12 N. Marcelino, J. Cernicharo, M. Agundez, E. Roueff, M. Gerin, J. Martin-Pintado, R. Mauersberger and C. Thum, *Astrophys. J.*, 2007, **665**, L127–L130.
- 13 N. Fourikis, M. W. Sinclair, B. J. Robinson, P. D. Godfrey and R. D. Brown, *Aust. J. Phys.*, 1974, **27**, 425–430.
- 14 M. B. Bell, H. E. Mathews and P. A. Feldman, *Astron. Astrophys.*, 1983, **127**, 420–422.
- 15 S. B. Charnley, *Adv. Space Res.*, 2004, **33**, 23.
- 16 M. Ikeda, M. Ohishi, A. Nummelin, J. E. Dickens, P. Bergman, A. Hjalmarson and W. M. Irvine, *Astrophys. J.*, 2001, **560**, 792–805.
- 17 B. E. Turner, *Astrophys. J., Suppl. Ser.*, 1991, **76**, 617–686.
- 18 J. N. Chengalur and N. Kanekar, *Astron. Astrophys.*, 2003, **403**, L43–L46.
- 19 B. E. Turner, R. Terziewa and E. Herbst, *Astrophys. J.*, 1999, **518**, 699–732.
- 20 E. Herbst and E. F. van-Dishoeck, *Annu. Rev. Astron. Astrophys.*, 2009, **47**, 427–480.
- 21 J. M. Hollis, F. J. Lovas and P. R. Jewell, *Astrophys. J.*, 2000, **540**, L107–L110.
- 22 D. T. Halfen, A. J. Apponi, N. Woolf, R. Polt and L. M. Ziurys, *Astrophys. J.*, 2006, **639**, 237–245.
- 23 M. T. Beltrán, C. Codella, S. Viti, R. Neri and R. Cesaroni, *Astrophys. J.*, 2009, **690**, L93–L96.
- 24 F. Combes, M. Gerin, A. Wooten, G. Włodarczyk, F. Clauset and P. J. Encrenaz, *Astron. Astrophys.*, 1987, **180**, L13–L16.
- 25 D. N. Friedel, L. E. Snyder, A. J. Remijan and B. E. Turner, *Astrophys. J.*, 2005, **632**, L95–L98.
- 26 J. M. Hollis, P. R. Jewell, F. J. Lovas, A. Remijan and H. Møllendal, *Astrophys. J.*, 2004, **310**, L21–L24.
- 27 B. E. Turner and A. J. Apponi, *Astrophys. J.*, 2001, **561**, L207–L210.
- 28 T. J. Millar and J. Hatchell, *Faraday Discuss.*, 1998, **109**, 15.
- 29 Y. C. Minh and E. F. van Dishoeck, *IAU Symp. 197, Astrochemistry: From Molecular Clouds to Planetary Systems*, San Francisco, 2000.
- 30 A. Bacmann, V. Taquet, A. Faure, C. Kahane and C. Ceccarelli, *Astron. Astrophys.*, 2012, **541**, L12.
- 31 A. Nummelin, J. E. Dickens, P. Bergman, A. Hjalmarson, W. M. Irvine, M. Ikeda and M. Ohishi, *Astron. Astrophys.*, 1998, **337**, 275–286.
- 32 A. G. G. M. Tielens and W. Hagen, *Astron. Astrophys.*, 1982, **114**, 245–260.
- 33 D. P. Ruffle and E. Herbst, *Mon. Not. R. Astron. Soc.*, 2001, **322**, 770–778.
- 34 P. Ehrenfreund and W. A. Schutte in *IAU Symp. 197, Astrochemistry: From Molecular Clouds to Planetary Systems*, 2000, p. 135.
- 35 E. L. Gibb, A. Nummelin, W. M. Irvine, D. C. B. Whittet and P. Bergman, *Astrophys. J.*, 2000, **545**, 309–326.
- 36 E. L. Gibb, D. C. B. Whittet, A. C. A. Boogert and A. G. G. M. Tielens, *Astrophys. J., Suppl. Ser.*, 2004, **151**, 35–73.
- 37 R. I. Kaiser and K. Roessler, *Astrophys. J.*, 1997, **475**, 144–154.
- 38 R. I. Kaiser and K. Roessler, *Astrophys. J.*, 1998, **503**, 959–975.
- 39 M. Garozzo, D. Fulvio, Z. Kanuchova, M. E. Palumbo and G. Strazzulla, *Astron. Astrophys.*, 2010, **509**, A67.
- 40 S. E. Bisschop, G. W. Fuchs, E. F. van-Dishoeck and H. Linnartz, *Astron. Astrophys.*, 2007, **474**, 1061.
- 41 W. D. Geppert, M. Hamberg, R. D. Thomas, F. Österdahl, F. Hellberg, V. Zhaunerchyk, A. Ehlerding, T. J. Millar, H. Roberts, J. Semaniak, M. af Ugglas, A. Källberg, A. Simonsson, M. Kaminska and M. Larsson, *Faraday Discuss.*, 2006, **133**, 177–190.
- 42 R. I. Kaiser, G. Eich, A. Gabrysch and K. Roessler, *Astrophys. J.*, 1997, **484**, 487–498.
- 43 C. J. Bennett, C. S. Jamieson, Y. Osamura and R. I. Kaiser, *Astrophys. J.*, 2005, **624**, 1097–1115.
- 44 C. J. Bennett, Y. Osamura, M. D. Lebar and R. I. Kaiser, *Astrophys. J.*, 2005, **634**, 698–711.
- 45 A. J. Apponi, D. T. Halfen, L. M. Ziurys, J. M. Hollis, A. J. Remijan and F. J. Lovas, *Astrophys. J.*, 2006, **643**, L29–L32.
- 46 M. D. Ward and S. D. Price, *Astrophys. J.*, 2011, **741**, 121.
- 47 B. M. Jones and R. I. Kaiser, *J. Phys. Chem. Lett.*, 2013, **4**, 1965.
- 48 C. J. Bennett, S. J. Brotton, B. M. Jones, A. K. Misra, S. Sharma and R. I. Kaiser, *Anal. Chem.*, 2013, **85**, 5659–5665.
- 49 M. S. Westley, G. A. Barattab and R. A. Baragiola, *J. Chem. Phys.*, 1998, **108**, 3321–3325.
- 50 C. J. Bennett, C. S. Jamieson, A. M. Mebel and R. I. Kaiser, *Phys. Chem. Chem. Phys.*, 2004, **6**, 735–746.
- 51 R. L. Hudson and M. H. Moore, *J. Geophys. Res.: Planets*, 2012, **106**, 33275–33284.
- 52 A. Wada, N. Mochizuki and K. Hiraoka, *Astrophys. J.*, 2006, 300–306.
- 53 R. Brunetto, G. Caniglia, G. A. Baratta and M. E. Palumbo, *Astrophys. J.*, 2008, **686**, 1480–1485.
- 54 D. Drouin, A. R. Couture, D. Joly, X. Tastet, V. Aimez and R. Gauvin, *Scanning*, 2007, **29**, 92–101.
- 55 G. Strazzulla, R. E. Johnson, R. L. Newburn, M. Neugebauer and J. Rahe, *Comets in the Post-Halley Era*, Springer, The Netherlands, 1991.
- 56 W. A. VonDrasek, S. Okajima and J. P. Hessler, *Appl. Opt.*, 1988, **27**, 4057–4061.
- 57 C. J. Bennett, C. S. Jamieson, Y. Osamura and R. I. Kaiser, *Astrophys. J.*, 2006, **653**, 792–811.

- 58 Y. S. Kim, C. J. Bennett, L. Sheng, K. O'Brien and R. I. Kaiser, *Astrophys. J.*, 2010, **711**, 744–756.
- 59 C. J. Bennett, C. S. Jamieson and R. I. Kaiser, *Phys. Chem. Chem. Phys.*, 2010, **12**, 4032–4050.
- 60 M. Hawkins and L. Andrews, *J. Am. Chem. Soc.*, 1983, **105**, 2523.
- 61 M. H. Moore and R. L. Hudson, *Icarus*, 2003, **161**, 486–500.
- 62 G. A. Guirgis, B. R. Drew, T. K. Gounev and J. R. Durig, *Spectrochim. Acta, Part A*, 1998, **54**, 123–143.
- 63 W. M. Coleman and B. M. Gordon, *Appl. Spectrosc.*, 1987, **41**, 1169–1172.
- 64 X. K. Zhang, E. G. Lewars, R. E. March and J. M. Parnis, *J. Chem. Phys.*, 1993, **97**, 4320–4325.
- 65 W. M. Coleman and B. M. Gordon, *Appl. Spectrosc.*, 1987, **41**, 1159–1161.
- 66 *Infrared and Raman Characteristic Group Frequencies*, ed. G. Socrates, John Wiley & Sons, Ltd, Chichester, 2001.
- 67 M. Frenklach, H. Wang and M. J. Roabinowitch, *Prog. Energy Combust. Sci.*, 1992, **19**, 47–73.
- 68 C. S. Jamieson, A. M. Mebel and R. I. Kaiser, *Astrophys. J., Suppl. Ser.*, 2006, **163**, 184–206.
- 69 W. Zheng, D. Jewitt and R. I. Kaiser, *Astrophys. J., Suppl. Ser.*, 2006, **648**, 753–761.
- 70 A. S. Wexler, *Appl. Spectrosc. Rev.*, 1967, **1**, 29–98.
- 71 J. Pearl, M. Ngoh, M. Ospina and R. Khanna, *J. Geophys. Res.: Planets*, 1991, **96**, 17477–17482.
- 72 NIST Chemistry WebBook.
- 73 R. I. Kaiser, P. Maksyutenko, C. Ennis, F. Zhang, X. Gu, A. M. Mebel, O. Kostko and M. Ahmed, *Faraday Discuss.*, 2010, **147**, Chemistry of the Planets.
- 74 L. Zhou, R. I. Kaiser, L. G. Gao, A. H. H. Chang, M. C. Liang and Y. Y. Yung, *Astrophys. J.*, 2008, **686**, 1493–1502.
- 75 C. J. Bennett, T. Hama, Y. S. Kim, M. Kawasaki and R. I. Kaiser, *Astrophys. J.*, 2011, **727**, 27–37.
- 76 C. J. Bennett, S. H. Chen, B. J. Sun, A. H. H. Chang and R. I. Kaiser, *Astrophys. J.*, 2007, **660**, 1588–1608.
- 77 B. M. Jones, C. J. Bennett and R. I. Kaiser, *Astrophys. J.*, 2011, **734**, 1–11.
- 78 S. L. W. Weaver and G. A. Blake, *Astrophys. J.*, 2005, **624**, L33–L36.
- 79 R. L. Hudson and M. J. Loeffler, *Astrophys. J.*, 2013, **77**, 109.
- 80 T. Shimanouchi, *Tables of Molecular Vibrational Frequencies Consolidated*, 1972, vol. I (NSRDS-NBs 39; Washington: National Bureau of Standards).